



SURFER v1.0: A flexible and simple model linking emissions to sea level rise

Marina Martínez Montero¹, Michel Crucifix¹, Victor Couplet¹, Nuria Brede^{2,4}, and Nicola Botta^{2,3}

¹Earth and Life Institute, UCLouvain, Louvain-la-Neuve, Belgium

²Potsdam Institute for Climate Impact Research, Potsdam, Germany

³Chalmers University of Technology, Göteborg, Sweden

⁴University of Potsdam, Potsdam, Germany

Correspondence: Marina Martínez Montero (marina.martinez@uclouvain.be)

Abstract. We present SURFER, a model for sea level rise that consists of three sub-models: an updated and expanded version of BEAM carbon cycle model (Glotter et al., 2014), a 2-box climate model that allows for solar radiation management and a simple ice sheet model that represents the tipping points and related timescales of Greenland and Antarctic ice sheets. The model, consisting of 8 ordinary differential equations, is fast, accurate up to timescales of several thousands of years and has been calibrated to reproduce results obtained by state of the art carbon cycle and ice sheet models. Additionally the ice sheet sub-model has been written in a flexible way that allows easily updating its parameters to match future results.

1 Introduction

Policy analysis and policy advice in the field of climate change is challenging and complex. Not only is it important to take into account up to date knowledge in climate science, but it is also important to be transparent and fair in the priorities and values that go into obtaining results used for advice.

A classical approach to policy advice is that of cost-benefit analysis where one proceeds by minimising a cost function — equivalently, maximising a utility function — such as to determine an optimal carbon tax, or answer questions like “what is the optimal way/path of reducing greenhouse gases (GHG) emissions in the next 100 years”. There has been a rising (but criticised, see (Gardiner, 2010)) interest for addressing the trade-offs associated with geoengineering mitigation options, such as to determine the “optimal mix of geoengineering and GHG emission reduction” (e.g., Moreno-Cruz and Keith, 2013; Helweggen et al., 2019). In that context, the “utility” is typically an aggregated quantity that somehow measures the world’s welfare¹, taking into account the costs of the different mitigation choices and the costs of damages due to climate change during the considered time-frame.

Most policy analyses put their focus on timescales of several decades to a couple of hundreds of years either by only looking at those timescales or by heavily discounting the future (e.g., Nordhaus, 1992; Moreno-Cruz and Keith, 2013; Helweggen et al., 2019; Hänsel et al., 2020), meaning that cost-benefit analyses are only performed taking into consideration the “close” future.

¹Not all studies maximise a single aggregated welfare quantity. In (Carlino et al., 2020), for example, the authors give optimal multi-objective policies with a time horizon of 500 years.



Additionally, the considered climate change damages are in general much lower than they should be, see (Keen, 2020; Keen et al., 2021) for an extensive critique. This is partly because only the damages from rising temperatures are considered, ignoring damages from ocean acidification, sea level rise and tipping points among others, and partly because of serious flaws present in the process of estimating the damages due to global warming.

It is disturbing that these studies focus on short-term periods given the well-known long residence time of carbon dioxide in the atmosphere-ocean system (Archer, 2005; Archer et al., 2009). Decisions about greenhouse gas emissions in the following decades to hundred years can have the potentially catastrophic consequences for climate and, in particular, sea level rise in the next thousands of years (e.g., Clark et al., 2016; Van Breedam et al., 2020). It is thus necessary to verify that optimal policies obtained with short-sighted analyses do not commit future generations to undesirable or even unmanageable situations. It would be even better to include such long-term effects in the policy analyses themselves.

State-of-the-art climate models are computationally too expensive to be used in policy analyses that explore many policy or control options, this is one reason why such analyses tend to rely on simplified models. Here we present a model for Sea-level Uprise Response under Forcings of Emissions and solar Radiation management (SURFER). SURFER is a light carbon-climate-ice sheets model that captures correctly timescales from decades to millennia providing melt rates for Greenland and Antarctic ice sheets in response to emissions of CO₂ that are compatible with state of the art ice sheet models.

Our objective is to provide a tool for assessing the long-term impacts of CO₂ emissions on sea level rise and ocean acidification. We show that SURFER's outputs are compatible with the latests emission driven experiments by Earth system Models of Intermediate Complexity (EMICs) and Earth System Models (ESMs), capturing well the responses of global mean surface temperature anomaly, atmospheric carbon concentration, sea level rise and also several metrics used to assess ocean acidification.

2 Model

SURFER consists of a system of 8 ordinary differential equations for the masses of carbon in four different reservoirs (atmosphere, upper ocean layer, deeper ocean layer and land), the temperature anomalies of two different reservoirs (upper ocean layer and deeper ocean layer), and the volume of Greenland and Antarctic ice sheets.

Two external forcings drive the system: anthropogenic CO₂ emissions and Solar Radiation Management in the form of SO₂ aerosol injections.

The CO₂ emission rate, through the accumulation of CO₂ in the atmosphere and due to the greenhouse effect, leads to long-lasting temperature increases, while the aerosol injections, through reflecting some of the incoming solar radiation, are responsible for fast but short-lasting temperature decreases. We refer the readers to (Moreno-Cruz and Keith, 2013; Helweggen et al., 2019) for more information on this form of geoengineering and to (Visoni et al., 2021) for the the latests results from the Geoengineering Model Inter-comparison Project. The CO₂ emissions are the source in the carbon cycle sub-model, which evolves the amount of carbon in the considered carbon reservoirs. The carbon concentration in the atmosphere and the aerosol injections are the driving forces of the climate sub-model, which evolves the temperature anomalies in two thermal reservoirs.

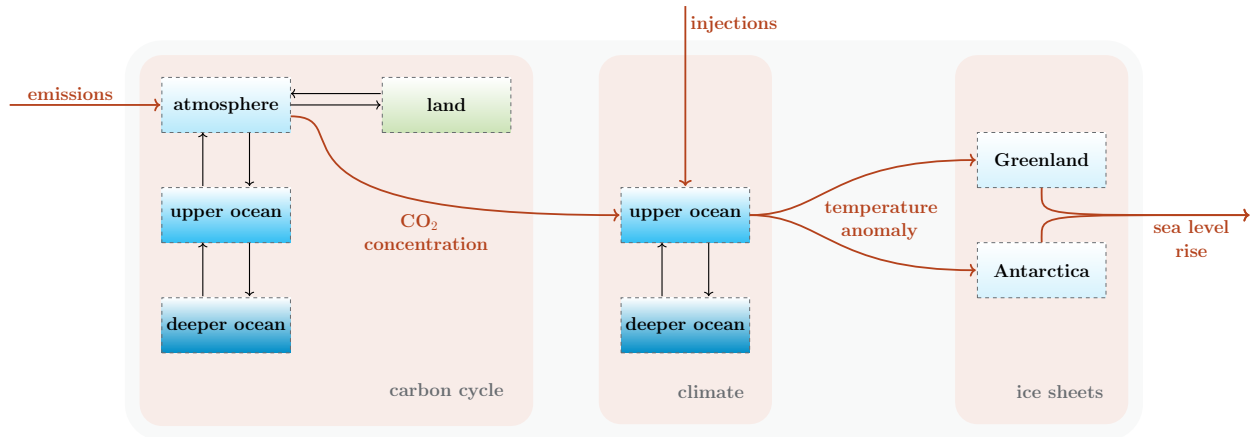


Figure 1. Conceptual diagram of SURFER. The state variables are indicated by the boxes, interactions and sources are depicted by black and dark orange arrows respectively.

55 Finally, the temperature anomaly of the upper ocean layer (assumed in equilibrium with the atmosphere and land) forces the melting of the ice sheets causing sea-level to rise. A conceptual diagram for the model can be found in Fig. 1. We have not included other interactions between the sub-models but we address the most relevant feedbacks in the discussion section.

2.1 Carbon cycle model

The carbon cycle model is based on BEAM, a simple carbon cycle model developed by Glotter et al. (2014) for economic and policy analyses. BEAM stands for “Bolin and Eriksson Adjusted Model” in acknowledgement of Bolin and Eriksson (1959). Since we modified the model by Glotter et al. (2014) by including an extra carbon reservoir, a land reservoir², along with minor modifications to the original equations, we proceed with a full presentation of the carbon cycle model.

The equations for the Atmosphere (A), upper ocean layer (U), deeper ocean layer (D) and land (L) carbon reservoirs read as follows

$$65 \quad \frac{dM_A}{dt} = E - F_{A \rightarrow U} - F_{A \rightarrow L}, \quad (1)$$

$$\frac{dM_U}{dt} = F_{A \rightarrow U} - F_{U \rightarrow D}, \quad (2)$$

$$\frac{dM_D}{dt} = F_{U \rightarrow D}, \quad (3)$$

$$\frac{dM_L}{dt} = F_{A \rightarrow L}, \quad (4)$$

²In Bolin and Eriksson (1959) they include hummus and vegetation reservoirs. We have followed a different approach for obtaining the equations and fluxes corresponding to the land reservoir.



where M_i is the mass of carbon in reservoir i , $F_{i \rightarrow j}$ the net carbon flux from reservoir i to reservoir j and E is the anthropogenic
 70 carbon emission rate. As part of the land reservoir we consider only soils and vegetation, ignoring carbon in permafrost and
 fossil fuel reserves. Sinks and sources associated with carbon outgassing, weathering and sediment burial are ignored because
 they are of secondary importance at the timescales considered here (10 yr to 5000 yr).

2.1.1 $F_{A \rightarrow U}$

Modelling the carbon flux between the atmosphere and the ocean relies on fundamental aspects of ocean carbonate chemistry
 75 which we now summarise (see chapter 8 of textbook by Sarmiento and Gruber (2006) for a deeper treatment).

When CO_2 in the atmosphere goes into the ocean it undergoes a series of chemical reactions



80 where H_2CO_3^* represents a mix of aqueous carbon dioxide, $\text{CO}_{2(\text{aqueous})}$, and carbonic acid, H_2CO_3 ³. The distribution be-
 tween the three carbon species H_2CO_3^* , HCO_3^- (bicarbonate), and CO_3^{2-} (carbonate), happens fast with respect to the ocean's
 circulation timescale, and hence equilibrium is assumed. The equilibrium distribution relations

$$K_1 = \frac{[\text{H}^+][\text{HCO}_3^-]}{[\text{H}_2\text{CO}_3^*]}, \quad K_2 = \frac{[\text{H}^+][\text{CO}_3^{2-}]}{[\text{HCO}_3^-]} \quad (5)$$

are dictated by the ocean's acidity, quantified by the proton concentration $[\text{H}^+]$. K_1 and K_2 are dissociation constants and
 85 $[\text{H}^+]$, measured in moles per kilogram, relates to the ocean pH as

$$\text{pH} = -\log_{10}[\text{H}^+]. \quad (6)$$

The total dissolved inorganic carbon (DIC) can then be written as

$$\begin{aligned} \text{DIC} &= [\text{H}_2\text{CO}_3^*] + [\text{HCO}_3^-] + [\text{CO}_3^{2-}] \\ &= \left(1 + \frac{K_1}{[\text{H}^+]} + \frac{K_1 K_2}{[\text{H}^+]^2} \right) [\text{H}_2\text{CO}_3^*]. \end{aligned} \quad (7)$$

90 In Fig. 2 we show the fractional contribution of the different carbon species to DIC for varying pH. For the present pH value
 of around 8 we can see in Fig. 2 that bicarbonate is the dominant carbon specie in the ocean. From the chemical reactions (R1),
 (R2) and (R3) we see that when CO_2 dissolves in the ocean, hydrogen ions are released and ocean acidifies. This in turn means
 that the proportion of carbonate decreases and that of H_2CO_3^* increases. The alkalinity however, defined as the excess of bases
 over acids

$$95 \quad Q = [\text{HCO}_3^-] + 2[\text{CO}_3^{2-}] + [\text{OH}^-] - [\text{H}^+] + [\text{B}(\text{OH})_4^-] + \text{minor bases}, \quad (8)$$

³It is common practice to consider these two species of carbon together into a single variable because they are difficult to distinguish from each other
 (Sarmiento and Gruber, 2006, Ch. 8.2).

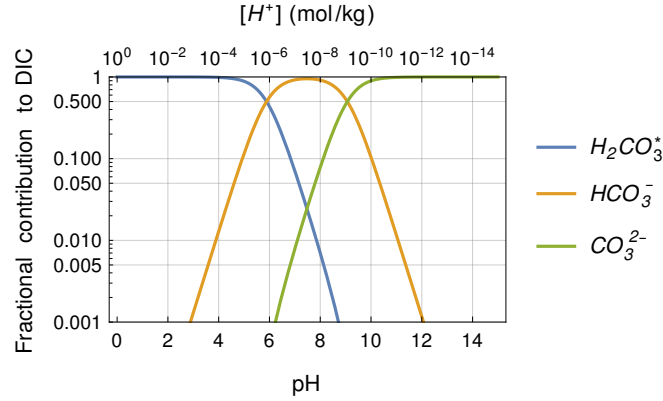


Figure 2. Carbon species fractional contribution to DIC for varying pH.

does not change with those reactions. Since no other reactions are accounted for in this carbon cycle model the alkalinity remains constant. This assumption will lead to stronger than expected acidification on long timescales (~ 4000 years) in which calcium carbonate production, dissolution and burial (not accounted for here) are significant. As it is usual practice, we will approximate the alkalinity⁴ by its dominant terms, that is by the carbonate alkalinity

$$100 \quad Q \approx [HCO_3^-] + 2[CO_3^{2-}] = \left(\frac{K_1}{[H^+]} + \frac{2K_1K_2}{[H^+]^2} \right) [H_2CO_3^*]. \quad (9)$$

The flow of CO_2 between the atmosphere and upper ocean layer is proportional to the difference in CO_2 partial pressures

$$F_{A \rightarrow U} \propto (p_{CO_2}^A - p_{CO_2}^U) \quad (10)$$

and by writing the partial pressures as proportional to the corresponding carbon masses

$$F_{A \rightarrow U} = -k_{A \rightarrow U} M_A + k_{U \rightarrow A} M_U' \quad (11)$$

105 where $p_{CO_2}^U$ refers to the partial pressure of carbon in the form $H_2CO_3^*$, and M_U' to the corresponding carbon mass. The parameters $k_{i \rightarrow j}$ are the transport coefficients from reservoir i to reservoir j .

The equilibrium concentration of $H_2CO_3^*$ in the ocean, corresponding to an atmospheric CO_2 partial pressure $p_{CO_2}^A$ can be determined through the CO_2 solubility constant

$$K_0 = \frac{[H_2CO_3^*]}{p_{CO_2}}, \quad (12)$$

110 where we have written p_{CO_2} without a reservoir index because in equilibrium atmospheric and upper ocean have the same CO_2 partial pressure.

⁴See e.g., Chapter 8 section 8.2 of Sarmiento and Gruber (2006) for more details on this.



2.1.2 $F_{U \rightarrow D}$

The exchange of carbon between the two ocean layers is ruled by oceanic currents and therefore depends on the total dissolved inorganic carbon in each layer

$$115 \quad F_{U \rightarrow D} = k_{U \rightarrow D} M_U - k_{D \rightarrow U} M_D. \quad (13)$$

This is in contrast with the carbon exchange between the upper ocean to atmosphere which depends on the upper ocean carbon concentration in the form of H_2CO_3^* . Now we can write the carbon cycle equations as

$$\frac{dM_A}{dt} = E - k_{A \rightarrow U} M_A + k_{U \rightarrow A} M'_U - F_{A \rightarrow L}, \quad (14a)$$

$$\frac{dM_U}{dt} = k_{A \rightarrow U} M_A - k_{U \rightarrow A} M'_U - k_{U \rightarrow D} M_U + k_{D \rightarrow U} M_D, \quad (14b)$$

$$120 \quad \frac{dM_D}{dt} = k_{U \rightarrow D} M_U - k_{D \rightarrow U} M_D, \quad (14c)$$

$$\frac{dM_L}{dt} = F_{A \rightarrow L}. \quad (14d)$$

Following Bolin and Eriksson (1959) we assume that the four reservoirs were in equilibrium in pre-industrial times (with $E(t_{PI}) = 0$) and we examine the equilibrium equations

$$125 \quad 0 = -k_{A \rightarrow U} M_A(t_{PI}) + k_{U \rightarrow A} M'_U(t_{PI}) - F_{A \rightarrow L}(t_{PI}), \quad (15a)$$

$$0 = k_{A \rightarrow U} M_A(t_{PI}) - k_{U \rightarrow A} M'_U(t_{PI}) - k_{U \rightarrow D} M_U(t_{PI}) + k_{D \rightarrow U} M_D(t_{PI}), \quad (15b)$$

$$0 = k_{U \rightarrow D} M_U(t_{PI}) - k_{D \rightarrow U} M_D(t_{PI}), \quad (15c)$$

$$0 = F_{A \rightarrow L}(t_{PI}). \quad (15d)$$

These allow to relate transport coefficients

$$130 \quad k_{A \rightarrow U} = k_{U \rightarrow A} \frac{M'_U(t_{PI})}{M_A(t_{PI})}, \quad (16)$$

$$k_{U \rightarrow D} = k_{D \rightarrow U} \frac{M_D(t_{PI})}{M_U(t_{PI})}, \quad (17)$$

where we can further write

$$M'_U = [\text{H}_2\text{CO}_3^*] W_U \bar{m}_C$$

$$M_A = \text{moles of CO}_2 \text{ in atmosphere} \times \bar{m}_C,$$

$$135 \quad M_{(U,D)} = \text{DIC}_{(U,D)} W_{(U,D)} \bar{m}_C,$$

where W_U and W_D stand for the whole mass of the upper and deeper ocean layers and can be approximated by

$$W_U \approx m_O \bar{m}_W \frac{h_U}{h_U + h_D}, \quad W_D \approx m_O \bar{m}_W \frac{h_D}{h_U + h_D}, \quad (18)$$



with m_O the moles of water in the ocean, \bar{m}_W the molar mass of H_2O , \bar{m}_C the molar mass of carbon and h_U and h_D the thicknesses of the ocean layers. Considering the equilibrium solubility relation (12) and

$$140 \quad p_{CO_2}^A = 1(\text{atm}) \frac{\text{moles of } CO_2 \text{ in atmosphere}}{\text{moles in atmosphere}}$$

we arrive at

$$k_{A \rightarrow U} = k_{U \rightarrow A} \frac{M'_U(t_{PI})}{M_A(t_{PI})} = k_{U \rightarrow A} \frac{W_U K_0}{m_A}, \quad (19)$$

$$k_{U \rightarrow D} = k_{D \rightarrow U} \frac{M_D(t_{PI})}{M_U(t_{PI})} = k_{D \rightarrow U} \delta_{DIC} \frac{h_D}{h_U}, \quad (20)$$

where m_A are the moles of air in the atmosphere and

$$145 \quad \delta_{DIC} = \frac{DIC_D(t_{PI})}{DIC_U(t_{PI})} \quad (21)$$

where $DIC_U(t_{PI})$ and $DIC_D(t_{PI})$ are the pre-industrial DIC concentration in upper and lower ocean layers. This parameter is a way to take into account the biological and carbonate pumps as it specifies the DIC gradient between the two ocean layers.

The next step is to express the carbon mass in $H_2CO_3^*$ form, M'_U , in Eqs. (14) as a function of the state variables. We begin by

$$150 \quad \frac{M'_U}{M_U} = \frac{[H_2CO_3^*]_U}{DIC_U} = \left(1 + \frac{K_1}{[H^+]_U} + \frac{K_1 K_2}{[H^+]_U^2} \right)^{-1}.$$

Using the definitions of DIC and carbonate alkalinity (Q in Eq. (9)), and the relation of DIC_i with carbon mass M_i , $[H^+]_i$ can be solved for in terms of M_i

$$[H^+]_i = \frac{K_1}{2\tilde{Q}_i} \left(\sqrt{(M_i - \tilde{Q}_i)^2 - 4 \frac{K_2}{K_1} \tilde{Q}_i (\tilde{Q}_i - 2M_i)} + (M_i - \tilde{Q}_i) \right) \quad (22)$$

with $i = U$ or D and where

$$155 \quad \tilde{Q}_i = Q_i W_i \bar{m}_C$$

is the carbon mass corresponding to the carbonate alkalinity. The factor tracking the ocean's buffer capacity becomes

$$B(M_U) \equiv \frac{M'_U}{M_U} = \frac{1}{2} - \frac{\tilde{Q}_U}{2M_U} + \frac{K_1 \sqrt{(M_U - \tilde{Q}_U)^2 - 4 \frac{K_2}{K_1} \tilde{Q}_U (\tilde{Q}_U - 2M_U)} - 4M_U K_2}{2M_U (K_1 - 4K_2)}. \quad (23)$$

2.1.3 $F_{A \rightarrow L}$

Now we turn to the equation for the land reservoir. The proposed equation is not process based, it is instead based on the output of the Zero Emissions Commitment Model Inter-comparison Project (ZECMIP) (Jones et al., 2019; MacDougall et al., 2020) experiments by different EMICs and ESMs.



We analysed the output of the ZECMIP experiments B1 and B3 in (Jones et al., 2019; MacDougall et al., 2020), and observed that the land carbon anomaly relaxes to a value proportional to the atmospheric carbon anomaly after typically 4 to 6 decades. This behaviour can be captured by the following relation:

$$165 \quad \delta M_L(t) = \alpha_L \delta M_A(t), \quad (24)$$

where $\delta M_i(t) = M_i(t) - M_i(t_{PI})$. The values of α_L approached by the different models in B1 experiments (lower cumulated emissions) tend to be higher than the ones approached by the higher cumulated emissions experiment B3. We noticed that the quantity

$$\frac{\delta M_L(t)}{\delta M_A(t)} \frac{M_A(t)}{M_A(t_{PI})} \quad (25)$$

170 tends to approach a model dependent constant value, say β_L , which is independent of the cumulated emissions after 4 to 6 decades. Based on these observations we propose the following equation for the land carbon anomaly δM_L

$$\frac{d\delta M_L}{dt} = k_{A \rightarrow L} \left(\beta_L \frac{M_A(t_{PI})}{M_A} \delta M_A - \delta M_L \right). \quad (26)$$

The final equations for the carbon cycle can now be written as

$$\frac{dM_A}{dt} = E(t) - k_{A \rightarrow U} \left(M_A - \frac{m_A}{W_U K_0} B(M_U) M_U \right) - k_{A \rightarrow L} \left(\beta_L M_A(t_{PI}) \left(1 - \frac{M_A(t_{PI})}{M_A} \right) - (M_L - M_L(t_{PI})) \right), \quad (27a)$$

$$175 \quad \frac{dM_U}{dt} = k_{A \rightarrow U} \left(M_A - \frac{m_A}{W_U K_0} B(M_U) M_U \right) - k_{U \rightarrow D} \left(M_U - \frac{1}{\delta_{DIC}} \frac{h_U}{h_D} M_D \right), \quad (27b)$$

$$\frac{dM_D}{dt} = k_{U \rightarrow D} \left(M_U - \frac{1}{\delta_{DIC}} \frac{h_U}{h_D} M_D \right), \quad (27c)$$

$$\frac{dM_L}{dt} = k_{A \rightarrow L} \left(\beta_L M_A(t_{PI}) \left(1 - \frac{M_A(t_{PI})}{M_A} \right) - (M_L - M_L(t_{PI})) \right). \quad (27d)$$

Equations (27) are very similar to the ones presented by Glotter et al. (2014) but with the following important differences:

1. There is a land carbon reservoir, this is an important update to the Glotter et al. (2014) model as it improves the agreement
180 with most recent results from EMICs and ESMs.
2. The ocean buffer factor is explicitly written in terms of M_U to highlight the non-linear nature of the model.
3. The relation between the transport coefficients between the two ocean layers here depends not only on the ratio of the thickness of the layers (δ) but also on the ratio of their pre-industrial concentration of dissolved inorganic carbon (δ_{DIC}). This allows for an equilibrium solution in which the dissolved inorganic carbon concentration is different in the upper and lower layer, which is known to be the case due to the soft tissue and carbonate pumps. Even if SURFER does not
185 explicitly consider those two pumps, including the pre-industrial DIC ratio of the two ocean layers yields better results for ocean acidification related quantities than assuming same carbon concentration at equilibrium.



The presented carbon cycle equations for atmosphere and ocean (and also the ones in Ref. Glotter et al. (2014)) look very similar to the ones considered in DICE, the Dynamic Integrated model of Climate and the Economy (Nordhaus, 1992, 2013).
 190 The big difference between the two is that the upper ocean buffer factor B is considered to be constant in DICE while in SURFER it evolves with the ocean acidification. By including the non-linearities due to ocean carbonate chemistry, SURFER's carbon cycle, as the one by Glotter et al. (2014), captures the fact that as the ocean takes in CO_2 from the atmosphere it becomes a worse sink for future CO_2 intake. This enables the correct tracking of carbon concentrations up to timescales of several thousands of years which is impossible with a linear model like DICE. One of the main objectives of the present
 195 contribution is to provide a model of sea level rise caused by ice sheet melting which is a slow process lasting several thousands of years. As explained by Archer et al. (2009), a linear carbon cycle is inadequate for such long-term purposes.

Another benefit of SURFER's carbon cycle is the tracking of the pH and the concentrations of the different carbon species in the ocean; this can be done a posteriori, using the obtained $M_U(t)$ together with Eqs. (22), (6), (9) and (5). SURFER can thus be of use for policy analyses that deal with ocean acidification.

200 Ocean acidification destabilises marine ecosystems making it more difficult for shellfish and corals to grow. As such, ocean acidification is one of the 9 identified planetary boundaries (Rockström et al., 2009; Steffen et al., 2015). This planetary boundary has however not been quantified in terms of pH, it is instead given in terms of the aragonite saturation state which can be approximated as

$$\Omega_{\text{ar}} \approx \frac{[\text{CO}_3^{2-}]}{[\text{CO}_3^{2-}]_{\text{saturation ar}}}, \quad (28)$$

205 where $[\text{CO}_3^{2-}]$ is the carbonate concentration in the ocean and $[\text{CO}_3^{2-}]_{\text{saturation ar}}$ is the carbonate concentration at which aragonite is saturated⁵. Aragonite is the most vulnerable form of calcium carbonate and its saturation state relates in a more straightforward way to some forms of marine life than pH. A value of $\Omega_{\text{ar}} < 1$ means that aragonite dissolves but organisms struggle to grow and thrive already at bigger values of Ω_{ar} . The planetary boundary is set at 80% of the pre-industrial value which was $\Omega_{\text{ar}}(t_{PI}) = 3.44$.

210 2.2 Climate model with solar radiation management

SURFER's climate sub-model is a linear 2-box model, similar to those in (Gregory, 2000; Held et al., 2010), for the evolution of the upper and deeper ocean temperature anomalies, δT_U and δT_D respectively

$$c_{\text{vol}} h_U \frac{d\delta T_U}{dt} = \beta \left(\frac{F(M_A, I)}{\beta} - \delta T_U \right) - \gamma (\delta T_U - \delta T_D), \quad (29)$$

$$c_{\text{vol}} h_D \frac{d\delta T_D}{dt} = \gamma (\delta T_U - \delta T_D). \quad (30)$$

215 The atmosphere is assumed to be in thermal equilibrium with the upper ocean layer. Due to this, and the fact that the upper ocean heat capacity is much bigger than that of the atmosphere, the atmosphere is not explicitly part of the climate sub-model and the radiative forcings are applied to the upper ocean layer. The constant c_{vol} is the seawater's volumetric heat capacity,

⁵ $[\text{CO}_3^{2-}]_{\text{saturation ar}}$ depends strongly on pressure and hence changes along the water column.



obtained by multiplying the specific heat capacity of seawater and the density of seawater. The thicknesses h_U and h_D of the two ocean layers are the same as for the carbon cycle. The thermal conductivity between the ocean layers is denoted by γ and β is the climate feedback parameter related to the equilibrium climate sensitivity

$$\text{ECS} = \frac{F_{2X}}{\beta}, \quad (31)$$

with F_{2X} the radiative forcing corresponding to a doubling of CO_2 . The anthropogenic radiative forcing in Eq. (29) responsible for the temperature anomalies consists of two terms,

$$F(M_A, I) = F_{2X} \log_2 \left(\frac{M_A}{M_A(t_{PI})} \right) - \alpha_{SO_2} \exp(-(\beta_{SO_2}/I)^{\gamma_{SO_2}}), \quad (32)$$

a first one corresponding to the standard greenhouse effect and a second one corresponding to solar radiation management in the form of aerosol injection. The solar radiation management term comes from (Niemeier and Timmreck, 2015). I corresponds to the sulfur injection rate and is in general time dependent.

2.3 Ice sheets and sea level rise

Multi-stability regions and tipping points have been identified both for the Greenland and Antarctic ice sheets (e.g., Lenton et al., 2008; Letreguilly et al., 1991; Pattyn, 2006; Ridley et al., 2010; Robinson et al., 2012; Gregory et al., 2020; Garbe et al., 2020). The proposed ice sheet model highlights those tipping points and is easy to adapt to capture the dynamics of these two ice sheets. The state variable is the volume fraction of ice with respect to a reference state, which we set to pre-industrial state. The sea level rise with respect to pre-industrial times is computed as a function of the ice sheets' melted fractions of ice and their total sea level rise potential.

To capture the dynamics of an ice sheet featuring multi-stability and tipping points we propose a non linear ordinary differential equation for the ice volume fraction

$$\frac{dV}{dt} = \mu(V, \delta T_U) (-V^3 + a_2 V^2 + a_1 V + c_1 \delta T_U + c_0), \quad (33)$$

where the third-order polynomial of the volume fraction and the term proportional to a forcing temperature imply a double fold bifurcation diagram for the steady states in terms of a constant forcing temperature, see Fig. 3. In contrast to the ocean part of the carbon cycle model and climate model presented before, the ice sheet model is not derived from physical processes; it is a generic dynamical system model based on the concept of a double-fold bifurcation calibrated on state-of-the-art ice sheet models' output. The constant parameters (a_2, a_1, c_1, c_0) are given in terms of the bifurcation points $((T_+, V_+), (T_-, V_-))$ as

$$a_2 = \frac{3(V_- + V_+)}{2}, \quad (34a)$$

$$a_1 = -3V_- V_+, \quad (34b)$$

$$c_1 = -\frac{(V_+ - V_-)^3}{2(T_+ - T_-)}, \quad (34c)$$

$$c_0 = +\frac{T_+ V_-^2 (V_- - 3V_+) - T_- V_+^2 (V_+ - 3V_-)}{2(T_- - T_+)}, \quad (34d)$$

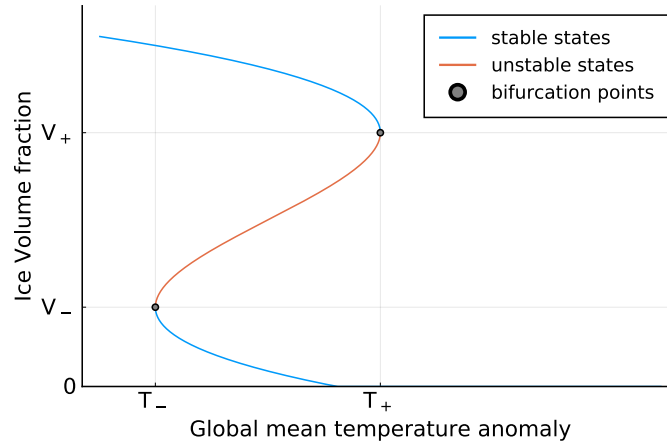


Figure 3. Ice sheet steady states for model defined in eqs. (33) and (34).

which are the quantities which determine the steady-state structure of the system, see Fig. 3. Since we want to impose the additional constraint of there existing a steady-state ice volume fraction of 1 at temperature anomaly equal to 0, the number of free parameters is reduced by one by setting

$$250 \quad V_- = \frac{-2 + V_+ (1 + G^{1/3} + G^{-1/3})}{-1 + G^{1/3} + G^{-1/3}} \quad (35)$$

with

$$G = \left(\frac{T_+ + T_- + 2\sqrt{T_- T_+}}{T_+ - T_-} \right). \quad (36)$$

Instead of fixing the 4 parameters $((T_+, V_+), (T_-, V_-))$ independently, V_- is given in terms of the other three such that the pre-industrial reference state condition $V_{eq}(\delta T_U = 0) = 1$ is satisfied.

255 The evolution is further affected by the forcing temperature δT_U and inverse timescale

$$\mu(V, \delta T_U) = \begin{cases} 1/\tau_+ & \text{if } H > 0, \\ 1/\tau_- & \text{if } H < 0 \text{ and } V > 0, \\ 0 & \text{if } H < 0 \text{ and } V = 0, \end{cases} \quad (37)$$

with

$$H = (-V^3 + a_2 V^2 + a_1 V + c_1 \delta T_U + c_0). \quad (38)$$

We write $\mu(V, \delta T_U)$ as a function of the state variables V and δT_U in such a way that it can take 3 different constant values.

260 This is done to reflect the fact that there is a timescale asymmetry between the processes of melting and freezing ice and to ensure that the ice fraction remains bigger or equal to zero.



2.4 Units, parameters and initial conditions

In this section we give the values and units of the parameters used to run the model. We also provide an explanation of how we have fixed some of them and obtained the pre-industrial initial conditions that we use in Sec. 3.

265 Parameters and initial conditions for the carbon cycle model can be found in Tables 1 and 2, the parameters for the climate model are in Table 3 and the ones for the ice sheet model (adapted to Greenland and Antarctica) can be found in Table 4. All examples in this paper will start from pre-industrial conditions, which for the climate and ice sheet models are trivial, $\delta T_{(U,D)}(t_{PI}) = 0$, $V_{(G,A)}(t_{PI}) = 1$.

2.4.1 Carbon cycle

270 The dissociation parameters K_1 and K_2 , the CO_2 solubility K_0 , and the alkalinity Q are assumed to be constant. A temperature (T) and salinity (S) dependent alternative is provided for K_1 , K_2 and K_0 in (Sarmiento and Gruber, 2006, Pg. 325)⁶. The specific values that we will be using for the constants K_1 , K_2 and K_0 have been obtained from the expressions in (Sarmiento and Gruber, 2006). We fix the parameter δ_{DIC} to 1.15 in accordance with data provided in (Sarmiento and Gruber, 2006, Pg. 320).

275 We fix the parameters K_1 , K_2 and K_0 in the carbon cycle model by ensuring that initial conditions are consistent with pre-industrial data. The parameter $\delta = h_D/h_U$, also playing a role in the initial conditions, has been set to $\delta = 20$, which is a middle ground between the thermal box sizes of (Gregory, 2000; Held et al., 2010) and the ratio of sizes suggested in (Bolin and Eriksson, 1959; Glotter et al., 2014), the reason for the chosen value is provided below. Other parameters, like $k_{A \rightarrow U}$, $k_{U \rightarrow D}$ and $k_{A \rightarrow L}$ have been adjusted to match the dynamics of more complex carbon cycle models. We now proceed with a
280 more in depth explanation.

In pre-industrial times the atmospheric CO_2 concentration was 280ppm which corresponds to an atmospheric carbon mass

$$\begin{aligned} M_A(t_{PI}) &= \text{moles of CO}_2 \text{ in atmosphere}(t_{PI}) \times \bar{m}_C \\ &= 280 \times 10^{-6} m_A \bar{m}_C = 580.3 \text{ PgC.} \end{aligned}$$

where \bar{m}_C is the Carbon molar mass. We assume that in pre-industrial conditions the carbon cycle was in equilibrium. Ad-
285 ditionally we impose that the total mass of carbon in the ocean was 38000 PgC. Using the relations between ocean carbon masses, the corresponding DICs and the equilibrium equations we can write

$$\begin{aligned} M_U(t_{PI}) + M_D(t_{PI}) &= \text{DIC}_U(t_{PI}) m_O \bar{m}_C \bar{m}_W \frac{1 + \delta_{\text{DIC}} \delta}{1 + \delta} \\ &= 38000 \text{ PgC} \end{aligned} \tag{39}$$

where we have written the carbon and water molar masses as $\bar{m}_{(C,W)}$. We see that $\delta = 20$ implies a reasonable value of
290 $\text{DIC}_U(t_{PI}) = 1973.53 \mu\text{mol kg}^{-1}$ ⁷.

⁶Similar expressions are given in Ref. Glotter et al. (2014)

⁷This value of DIC is one of the ingredients used to fix the dissociation and solubility constants



The pH of the upper ocean in pre-industrial times was around 8.2. Here we will fix it to 8.17 in accordance to historical CMIP6 results in (Gutiérrez et al., 2021) which implies a Hydrogen ion concentration of $[\text{H}^+](t_{PI}) = 10^{-8.17} \text{ mol kg}^{-1}$. Q_U and DIC_U at pre-industrial time can be written as

$$Q_U = \left(\frac{K_1}{[\text{H}^+](t_{PI})} + \frac{2K_1K_2}{([\text{H}^+](t_{PI}))^2} \right) K_0 p_{\text{CO}_2}^A(t_{PI}),$$

$$295 \quad \text{DIC}_U(t_{PI}) = \left(1 + \frac{K_1}{[\text{H}^+](t_{PI})} + \frac{K_1K_2}{([\text{H}^+](t_{PI}))^2} \right) K_0 p_{\text{CO}_2}^A(t_{PI})$$

where $p_{\text{CO}_2}^A(t_{PI}) = 280 \times 10^{-6} \text{ atm}$. We use these relations to fix the dissociation and solubility constants. First, we impose an alkalinity value compatible with observations $Q_U = 2200 \mu\text{mol kg}^{-1}$. Second, we impose the already fixed value of $\text{DIC}_U(t_{PI}) = 1973.53 \mu\text{mol kg}^{-1}$. Third, we use the temperature (T) and salinity (S) dependent expressions for the dissociation and solubility given in (Sarmiento and Gruber, 2006). Last, we solve the system of two equations for T and S numerically.
 300 Such a procedure yields “effective” $T = 294.7\text{K}$ and $S = 32.49\%$ a warmer and slightly less salty ocean than the global averages, but they determine dissociation constants which, in the end, yield realistic carbon masses, concentrations, and alkalinity in the pre-industrial ocean.

We ignore the temperature dependence of the carbonate concentration corresponding to aragonite saturation and we fix it to

$$[\text{CO}_3^{2-}]_{\text{saturation ar}} = \frac{[\text{CO}_3^{2-}](t_{PI})}{\Omega_{\text{ar}}(t_{PI})} \quad (40)$$

305 where $[\text{CO}_3^{2-}](t_{PI})$ is obtained through Eqs. (5) and (12) and $\Omega_{\text{ar}}(t_{PI}) = 3.44$ from (Rockström et al., 2009; Steffen et al., 2015).

The ZECMIP B1 and B3 experiments outputs suggest a land carbon parameter β_L between 0.5 and 2.3 We settled for 1.7 but the choice is not critical. The pre-industrial mass of land carbon is set to 2200 PgC for plotting purposes but this quantity does not affect the land carbon uptake.

310 Finally, for the inverse timescale $k_{A \rightarrow U}$ we kept the value recommended by Glotter et al. (2014). $k_{U \rightarrow D}$ was fixed to obtain a timescale for the deep ocean dynamics of 1000 years $k_{U \rightarrow D} = \delta \delta_{\text{DIC}}/1000$. The inverse timescale $k_{A \rightarrow L}$ was fixed to match the output of ZECMIP B1 and B3 experiments.

Users of the model are invited to explore other possibilities of fixing parameters but in this paper we will restrict ourselves to using SURFER only with the supplied parameters and initial conditions and we will show that, despite its simplicity, its
 315 predictions are in excellent agreement with more complex models.

2.4.2 Climate

In the climate model we need to fix the parameters h_U (or h_D , since the ratio δ has already been fixed), c_{vol} , F_{2X} , β , γ , and the parameters from the aerosol forcing α_{SO_2} , β_{SO_2} , γ_{SO_2} . The values adopted in the following are listed on Table 3.

320 The sea water volumetric heat capacity c_{vol} is obtained by multiplying the specific heat capacity of seawater, which is taken to be $3850 \text{ J kg}^{-1} \text{ }^\circ\text{C}^{-1}$ and the density of seawater, taken to be 1027 kg m^{-3} . The extra radiative forcing due to a doubling



Quantity	Value
δ	20
δ_{DIC}	1.15
K_0	$3.148 \times 10^{-2} \text{ mol (kg atm)}^{-1}$
K_1	$1.326 \times 10^{-6} \text{ mol kg}^{-1}$
K_2	$9.198 \times 10^{-10} \text{ mol kg}^{-1}$
m_A	$1.727 \times 10^{20} \text{ mol}$
m_O	$7.8 \times 10^{22} \text{ mol}$
\bar{m}_C	$12 \times 10^{-3} \text{ kg mol}^{-1}$
\bar{m}_W	$18 \times 10^{-3} \text{ kg mol}^{-1}$
Q_U	$2.2 \times 10^{-3} \text{ mol kg}^{-1}$
\tilde{Q}_U	1765.0 PgC
$[\text{CO}_3^{2-}]_{\text{saturation ar}}$	$68.40 \mu\text{mol kg}^{-1}$
$k_{A \rightarrow U}$	0.25 yr^{-1}
$k_{U \rightarrow D}$	0.023 yr^{-1}
$k_{U \rightarrow L}$	0.025 yr^{-1}
β_L	1.7

Table 1. Values of parameters for the carbon cycle model.

Quantity	Value
$M_A(t_{PI})$	580.3 PgC
$M_U(t_{PI})$	1583.3 PgC
$M_D(t_{PI})$	36416.7 PgC
$M_L(t_{PI})$	2200 PgC

Table 2. Initial equilibrium pre-industrial conditions obtained for the parameters specified in Table 1.

concentration of CO_2 , F_{2X} , comes from the 6th IPCC Assessment Report (Arias et al., 2021) and parameter h_U comes from (Gregory, 2000). β and γ have been fixed to yield Equilibrium Climate Sensitivity and Transient Climate Response

$$\text{ECS} = \frac{F_{2X}}{\beta} = 3.5, \quad \text{TCR} = \frac{F_{2X}}{\beta + \gamma} = 2.0, \quad (41)$$



compatible with results in the 6th IPCC Assessment Report (Arias et al., 2021), i.e., ECS very likely [2 to 5] °C and TCR very likely [1.4 to 2.2] °C . Aerosol forcing parameters come from the work of Niemeier and Timmreck (2015).

Parameter	Value(s)
F_{2X}	3.9 W m ⁻²
β	1.1143 W m ⁻² °C ⁻¹
γ	0.8357 W m ⁻² °C ⁻¹
h_U	150 m
h_D	3000 m
c_{vol}	0.13 W yr m ⁻³ °C ⁻¹
α_{SO_2}	65 W m ⁻²
β_{SO_2}	2246 TgS yr ⁻¹
γ_{SO_2}	0.23

Table 3. Values of parameters for the temperature module.

325

2.4.3 Ice sheets

We now proceed to fix the values of the parameters $(T_+, T_-, V_+, \tau_+, \tau_-)$ ⁸ for adapting the ice sheet model to Greenland and Antarctica, see Table 4.

For Greenland, we have fixed the bifurcation points (T_{\pm}, V_+) and the melting timescale τ_- by fitting SURFER to the results of Robinson et al. (2012)⁹; to fix τ_+ we have instead looked at the timescales that appear on the freezing experiments in (Letreguilly et al., 1991; Pattyn, 2006). For the case of Antarctica we have relied on two references, Garbe et al. (2020); Van Breedam et al. (2020), to fix (T_{\pm}, V_+, τ_-) ; the first one containing steady state experiments and the second one dynamical experiments. The parameter τ_+ has been fixed by fitting to the results of (Pattyn, 2006; Huybrechts, 1993). Greenland's and Antarctic's ice sheet SLR potential, linking the ice volume fraction to an eustatic sea-level rise, come from (Van Breedam et al., 2020) and (Garbe et al., 2020) respectively.

335

Again, SURFER is intended to be tuned on state-of-the art models. Its parameters can, therefore, be revised as new simulations become available.

⁸The parameter V_- has been fixed by using Eq. (35).

⁹Notice that δT_U is the global mean temperature anomaly and that their plots are for regional summer temperature anomaly. On their supplementary information they explain how to relate the two.



Parameter	Greenland's value	Antarctica's value
T_+	1.6 °C	6.8 °C
T_-	0.4 °C	5.5 °C
V_+	0.77	0.55
V_-	0.3649	0.108
τ_+	5500 yr	5500 yr
τ_-	400 yr	500 yr
SLR potential	7.4 m	55 m

Table 4. Values of parameters used here for Greenland and Antarctic ice sheets.

2.5 Numerics

The model has been implemented in The Julia Programming Language (Bezanson et al., 2017) in the jupyter-lab environ-
340 ment. The equations have been integrated using the package `DifferentialEquations.jl` with the integration method
`Rosenbrock23()` with `abstol=1e-12` and `reltol=1e-3`. The model runs extremely fast, each run of up to 10000
years taking ≈ 0.003 seconds on a laptop with processor Intel® Core™ i7-9850H CPU @ 2.60GHz $\times 12$.

3 Showcasing the model

In this section we show the model's behaviour when forced by different CO₂ emission scenarios. Whenever it has been possible
345 to retrieve outputs of other models we have done so for making the comparison easier.

3.1 ZECMIP B1 and B3 experiments

The ZECMIP B1 and B3 experiments (Jones et al., 2019; MacDougall et al., 2020) consist in starting with pre-industrial
conditions and forcing the system with the bell shaped emission curves in Fig. 4 corresponding to 1000 PgC cumulated
emissions for the B1 experiment and 2000 PgC for the B3 experiment. We consider the output of 6 EMICs and 2 ESMs
350 that participated in the ZECMIP experiment. The EMICs are Bern3D-LPX-ECS3K, DCESS1.0, MESM, MIROC-lite-LCM,
PLASIM-GENIE, UVicESCM2.10 and the ESMs are GFDL-ESM2M and NorESM2-LM. Figures 5 and 6 show the good
agreement of SURFER's output to that of the ZECMIP experiments. SURFER's land model is closer to the ESMs than the
EMICs although this can be changed by tuning β_L on the carbon cycle equations.

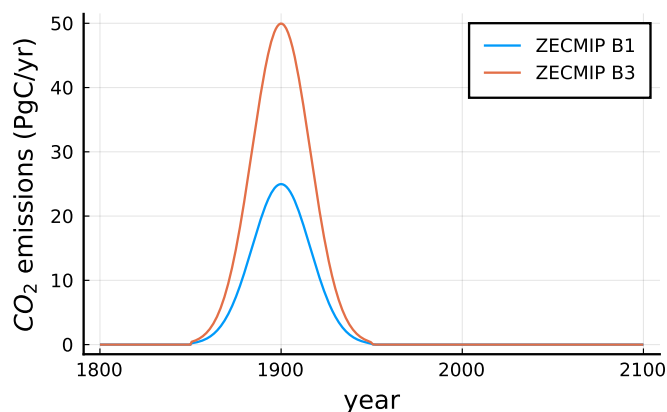


Figure 4. CO₂ emission curves for ZECMIP experiments B1 and B3.

3.2 Ocean acidification under RCP or SSP forcing scenarios

355 In this section we run SURFER forced with historic CO₂ emissions followed by CO₂ emissions associated to the Representative
 Concentration Pathways (RCPs) and Shared Socio-economic Pathways (SSPs) together with their extensions (Meinshausen
 et al., 2011, 2020)¹⁰, see Fig. 7. For the RCPs emission scenarios we have considered, as Van Breendam et al. (2020), that CO₂
 emissions are zero from 2300 onwards. For the SSPs emission scenarios, as in (Meinshausen et al., 2020), we consider that
 CO₂ emissions are zero from 2250. We have considered that the Solar Radiation Management sulphur injections remain zero
 360 during the whole simulation period.

Figure 8 shows the evolution of different variables when forced by these scenarios. As CO₂ is emitted into the atmosphere,
 the CO₂ concentration in the atmosphere rises and so does the temperature and the DIC in the ocean's upper layer. Together
 with the increase in DIC, the pH, carbonate concentration and aragonite saturation state decrease. For the aragonite saturation
 state $(\Omega_{ar})_U$, in Fig. 8, we have shadowed the region beyond the planetary boundary for ocean acidification. SURFER predicts
 365 that all considered emission scenarios cross that planetary boundary. Scenarios RCP8.5, SSP5-8.5 and SSP3-7 reach values of
 aragonite saturation state smaller or close to 1; in those scenarios aragonite would dissolve in the upper ocean.

Figure 9 compares SURFER's pH prediction to that of CMIP5 and CMIP6 shown in (Kwiatkowski et al., 2020). SURFER
 exhibits more acidification than CMIP5 and CMIP6 but it is in better agreement with CMIP6 runs.

3.3 Sea level rise in extended RCP scenarios

370 In this section we show the long-term model's behaviour when forced by historic anthropogenic CO₂ emissions followed by
 the extended RCPs emission scenarios, see (Moss et al., 2010; Meinshausen et al., 2011), which we continue to extend from
 the year 2300 onwards with zero emissions, as in (Van Breendam et al., 2020), see Fig. 7.

¹⁰For the SSPs we were only able to find the emission data up to 2100. We modelled the extension with a linear function going to zero by 2250. This is
 what was done by Meinshausen et al. (2020) except for the lowest emission scenario SSP1-2.6.

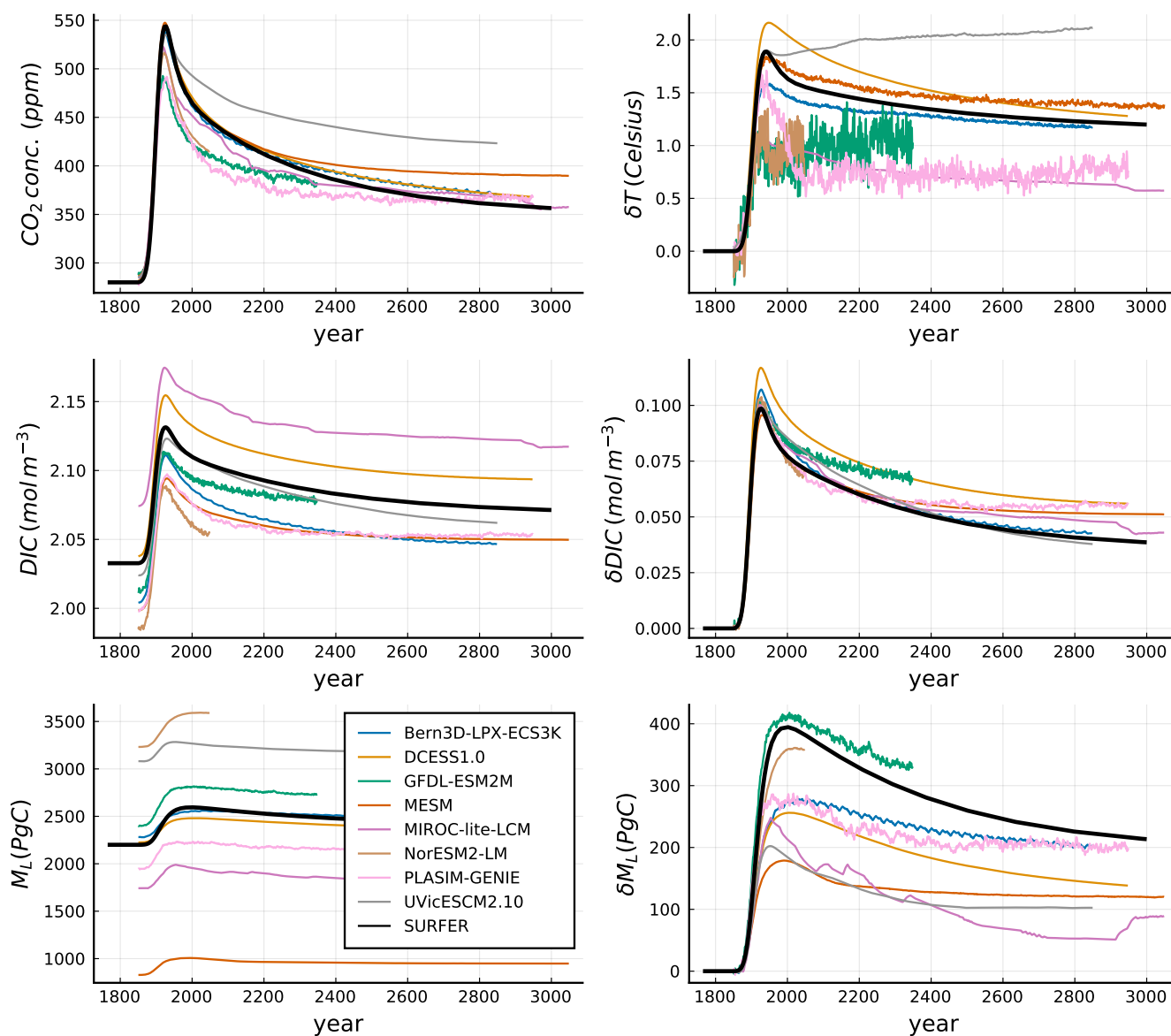


Figure 5. ZECMIP B1 experiment outputs of 6 EMICs, 2 ESMs and SURFER. From left to right, top to bottom: CO₂ concentration in the atmosphere, atmospheric global mean temperature anomaly, dissolved inorganic carbon in the upper layer, dissolved inorganic carbon anomaly in the upper layer, total of carbon in the land reservoir and carbon anomaly in land reservoir.

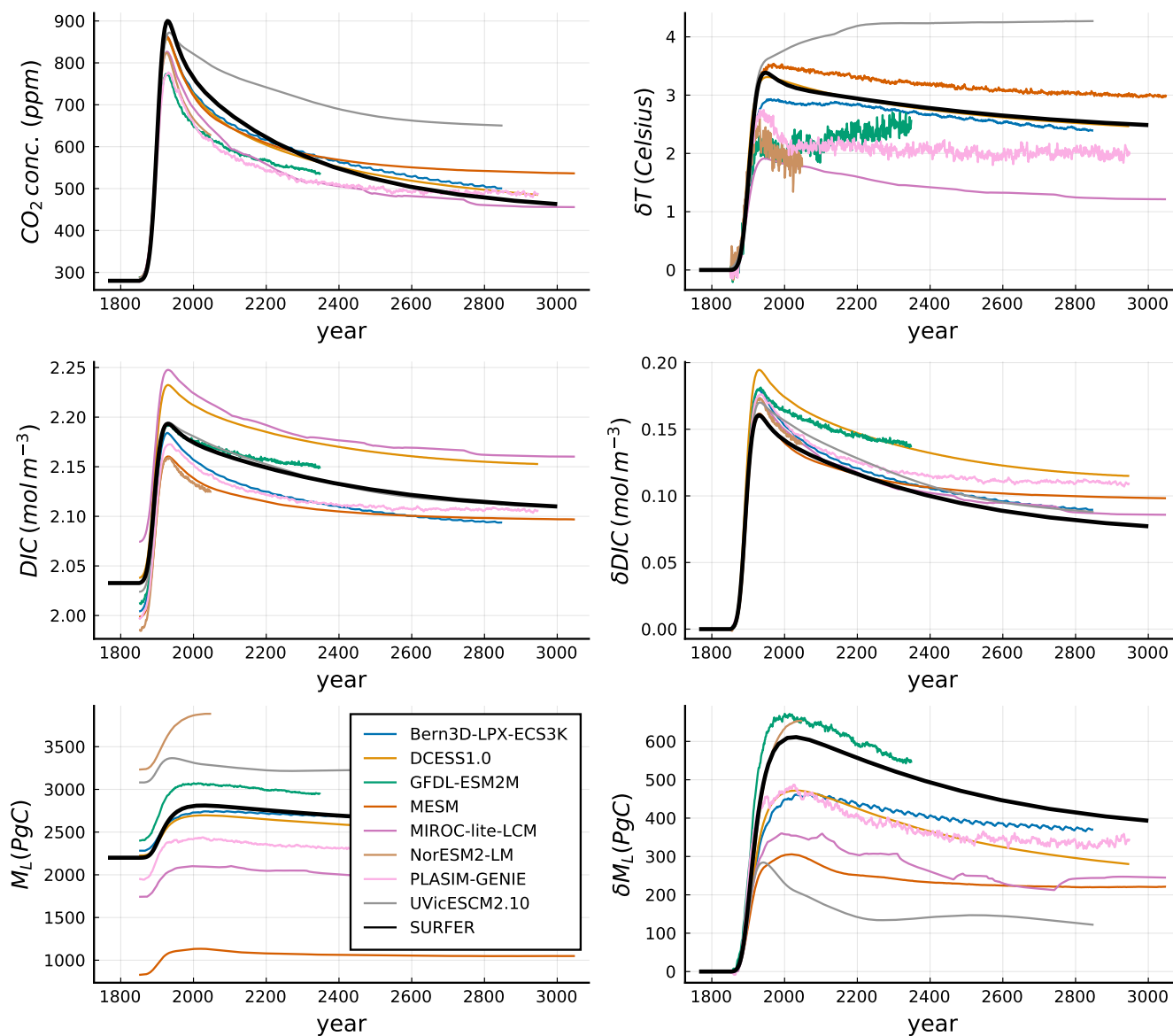


Figure 6. ZECMIP B3 experiment outputs of 6 EMICs, 2 ESMs and SURFER.. From left to right, top to bottom: CO₂ concentration in the atmosphere, atmospheric global mean temperature anomaly, dissolved inorganic carbon in the upper layer, dissolved inorganic carbon anomaly in the upper layer, total of carbon in the land reservoir and carbon anomaly in land reservoir.

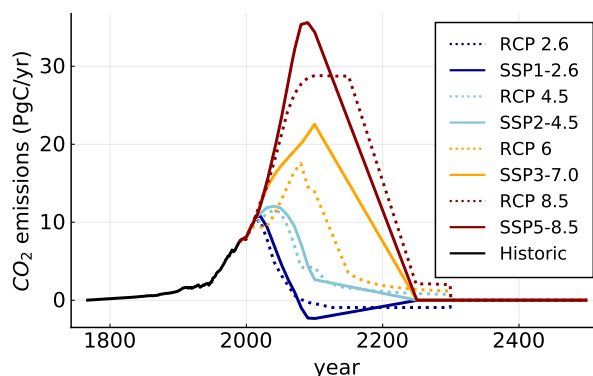


Figure 7. CO₂ emission rate for the RCP and SSP scenarios with their extensions.

Simulations were started from pre-industrial conditions considering an initial volume fraction of 1 for both ice sheets. Solar Radiation Management sulfur injections remain zero during the whole simulation period.

375 Figure 10 shows the behaviour of some of the tracked variables for a period of 10000 years. Due the absence of calcium carbonate reactions in the carbon sub-model and the fact that SURFER does not include any feedback from the ice sheet melting on the temperature, quantities from the carbon cycle and climate sub-models have reached equilibrium around year 6000. After that time only the ice sheet components of the model continue to evolve. If carbonate compensation was included, a slow lowering of the atmospheric CO₂ concentration and temperature would be observed, together with its corresponding
 380 effect on the ice sheets¹¹. Albedo feedbacks of the ice sheets on the climate sub-model would act in the opposite direction increasing the temperature. These effects, as mentioned in the discussion session, are expected to be relatively small.

The agreement of the sea level rise plot, Fig. 10, with the results shown in Fig. 5 of (Van Breedam et al., 2020) is good, specially for the Antarctic ice sheet. The agreement for the Greenland's ice sheet is not as good, specially for the two lowest forcing scenarios. The reason for this is that we fixed Greenland's parameters according to the results of Robinson et al. (2012)
 385 and that the tipping points do not exactly coincide; Greenland's ice sheet in (Robinson et al., 2012), and hence SURFER's, seems to have a higher temperature tipping point than the one of in (Van Breedam et al., 2020). SURFER can also track the sea level rise rate, see Fig. 10, a quantity that plays a crucial role in the context of adaptation to sea level rise. Greenland completely melts around the year 5000 for scenario RCP-8.5, this explains the small but sharp drop in the rate of sea level rise around the same time for the corresponding scenario.

390 3.4 Solar radiation management

As a last example we perform an experiment done by the Geoengineering Model Inter-comparison project and compare SURFER's output to their results. We focus on the G6sulfur experiment introduced in (Kravitz et al., 2015). In the G6sulfur

¹¹We expect this effect to be small because most of the ice sheet melting occurs in the first thousands of years where carbonate compensation still plays a very subdominant role.

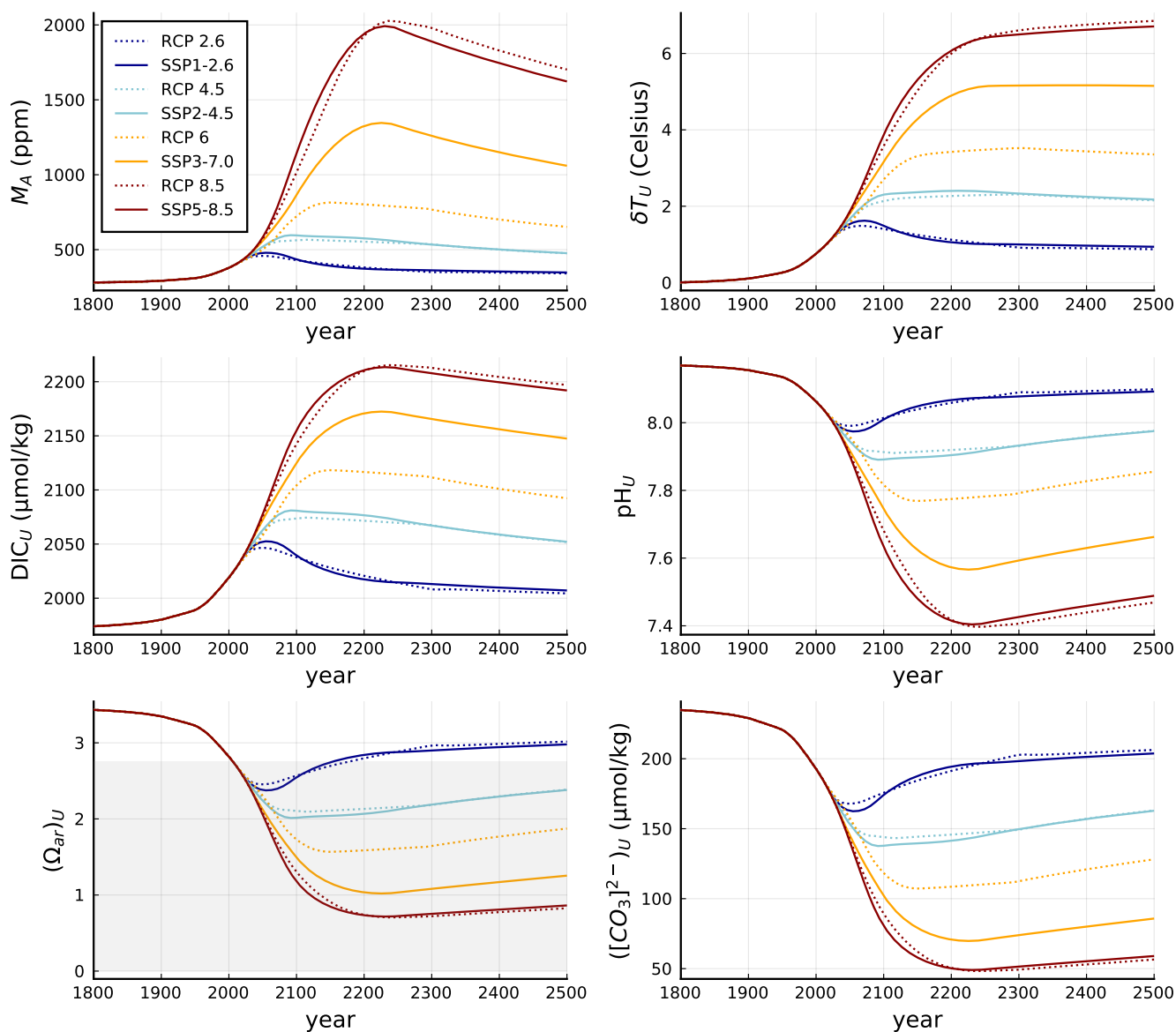


Figure 8. SURFER’s output when forced by the extended RCPs and SSPs emission scenarios. From left to right, top to bottom: atmospheric CO₂ concentration, global mean temperature anomaly, Dissolved Inorganic Carbon in the upper layer, pH in the upper layer, aragonite saturation state in the upper layer and carbonate concentration in the upper layer.

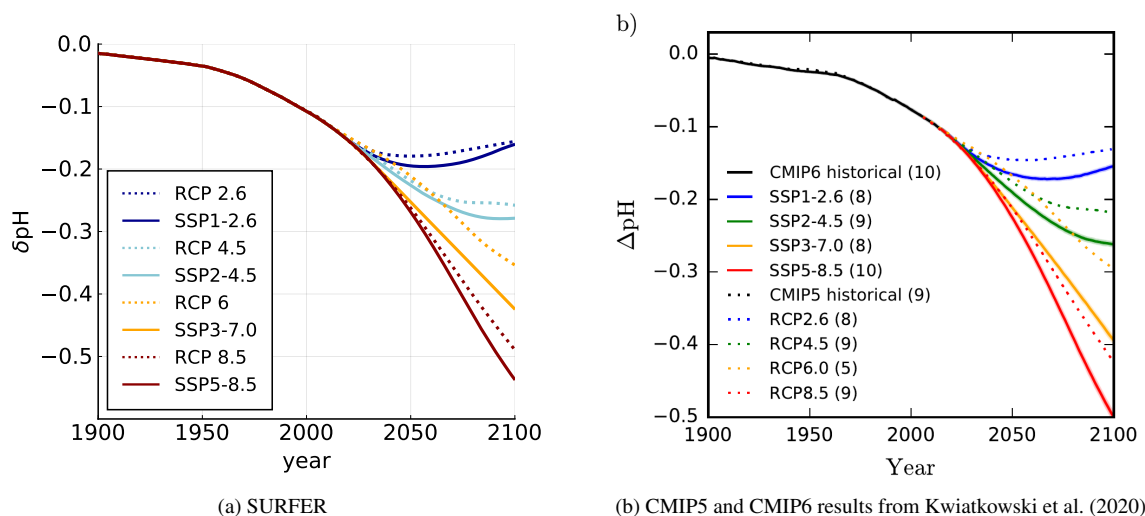


Figure 9. Change in pH in the upper ocean layer under RCPs and SSPs emission scenarios.

experiment, stratospheric aerosols are injected into the model with the goal of reducing the magnitude of the net anthropogenic radiative forcing from a high forcing scenario (SSP5-8.5) to match that of a medium forcing scenario (SSP2-4.5).

395 We run SURFER forced by the CO₂ emissions corresponding to the SSP scenarios SSP5-8.5 and SSP2-4.5 in the absence of solar radiation management. We compute the radiative forcing difference between the two scenarios, and we perform a third run in which SURFER is forced by the CO₂ emissions corresponding to scenario SSP5-8.5 and with sulfur aerosol injections exactly compensating the extra radiative forcing in SSP5-8.5 with respect to SSP2-4.5

$$I(t) = \beta_{SO_2} \left(-\log \left(\frac{F^{(SSP5-8.5)}(t) - F^{(SSP2-4.5)}(t)}{\alpha_{SO_2}} \right) \right)^{1/\gamma_{SO_2}} \quad (42)$$

400 with $F^{(SSP2-4.5)}$ and $F^{(SSP2-4.5)}$ the time varying radiative forcing obtained under the corresponding scenarios.

Figure 11 shows SURFER predictions for CO₂ concentration, radiative forcing, temperature and pH of upper ocean layer. This shows that while the radiative forcing, and hence the temperature, is lowered by the injection of aerosols, the high CO₂ concentration and ocean acidification related problems remain. In Figure 12 we compare the rate of sulfur injections needed by SURFER and by the ESMs that participated in the GeoMIP to accomplish the G6sulfur experiment.

405 4 Discussion

SURFER is simple, easy to understand and fast to run, but it misses some processes, carbon reservoirs and feedbacks. This gives room for extensions, and here we provide relevant information for users who would like to take some of the relevant processes into account, while explaining why we have not included them in the present model.

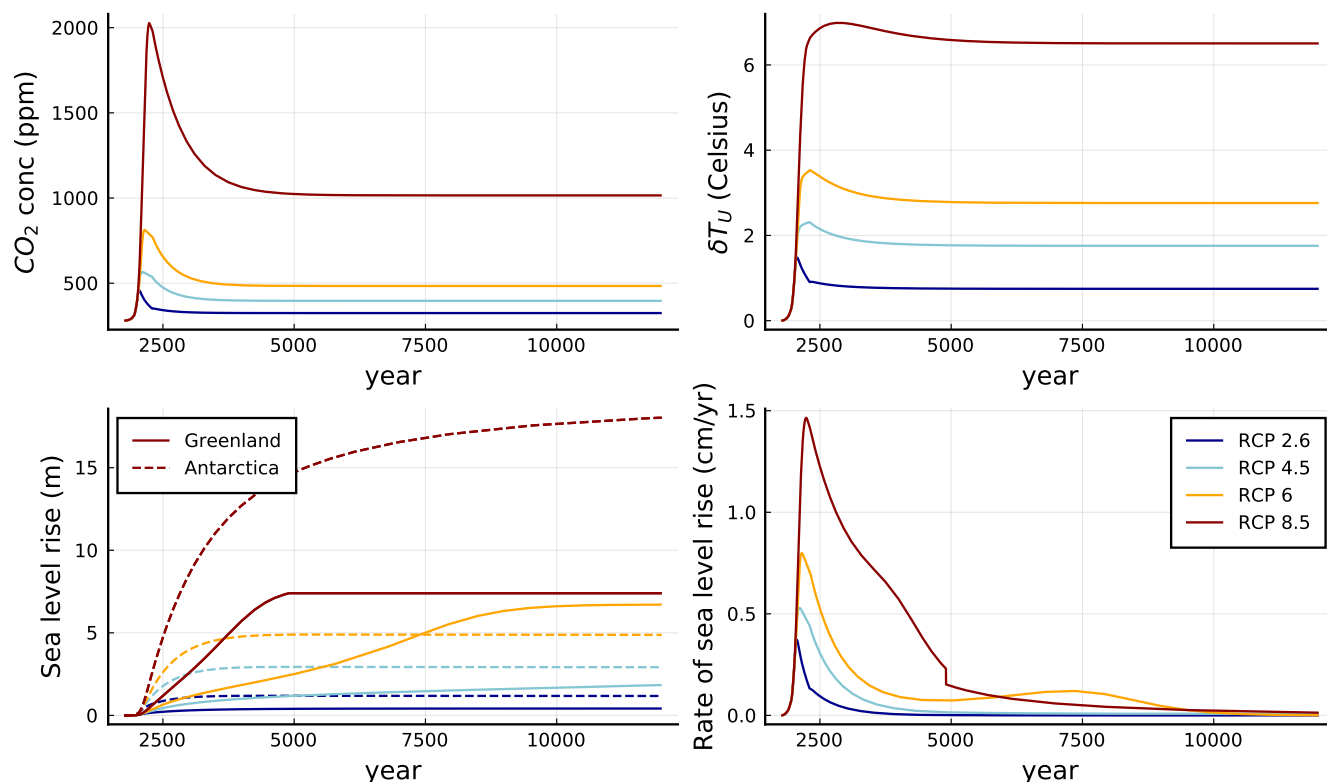


Figure 10. Long time behaviour of some of SURFER’s variables when forced by RCP scenarios. From left to right, top to bottom: CO₂ concentration, upper ocean temperature anomaly, cumulative sea level rise, sea level rise rate. The cumulative sea level rise plot shows contributions from Greenland and Antarctic ice sheets separately, indicated by solid and dashed lines respectively. The rate of sea level rise plot shows their joint contribution.

Permafrost holds approximately 1400 PgC (Canadell et al., 2021): that is about twice as much carbon as currently contained
 410 in the atmosphere. The thawing and subsequent release of part of that carbon into the atmosphere may therefore constitute a
 substantial positive feedback on anthropogenic emissions. Several studies, simulations and observations have been made to
 quantify the strength of these effects, (MacDougall and Knutti, 2016; Chadburn et al., 2017; Burke et al., 2017; Turetsky et al.,
 2020; Burke et al., 2020) but the spread in the estimates is considerable. MacDougall and Knutti (2016) made projections of
 the release of carbon from permafrost soils using a perturbed parameter ensemble with the UVic-ESCM EMIC. Among other
 415 things, they computed the sensitivities of cumulative emitted carbon per extra degree of warming. They showed the (transient)
 sensitivities changed with time, obtaining 24, 39, and 47 PgC/°C for the years 2100, 2200 and 2300 under all RCP scenarios.
 A similar computation was done by Burke et al. (2017) with the IMOGEN model coupled to two different land models. In that
 case, although lower values were obtained, the sensitivities remained time dependent (~ 10, 20, 30 PgC/°C for 2100, 2200
 and 2300 under all RCP scenarios). In an observation-based study, Chadburn et al. (2017) estimated an equilibrium sensitivity
 420 of permafrost area loss per degree of future global warming of $4.0_{-1.1}^{+1.0}$ million km²/°C. The climatic consequences for CO₂

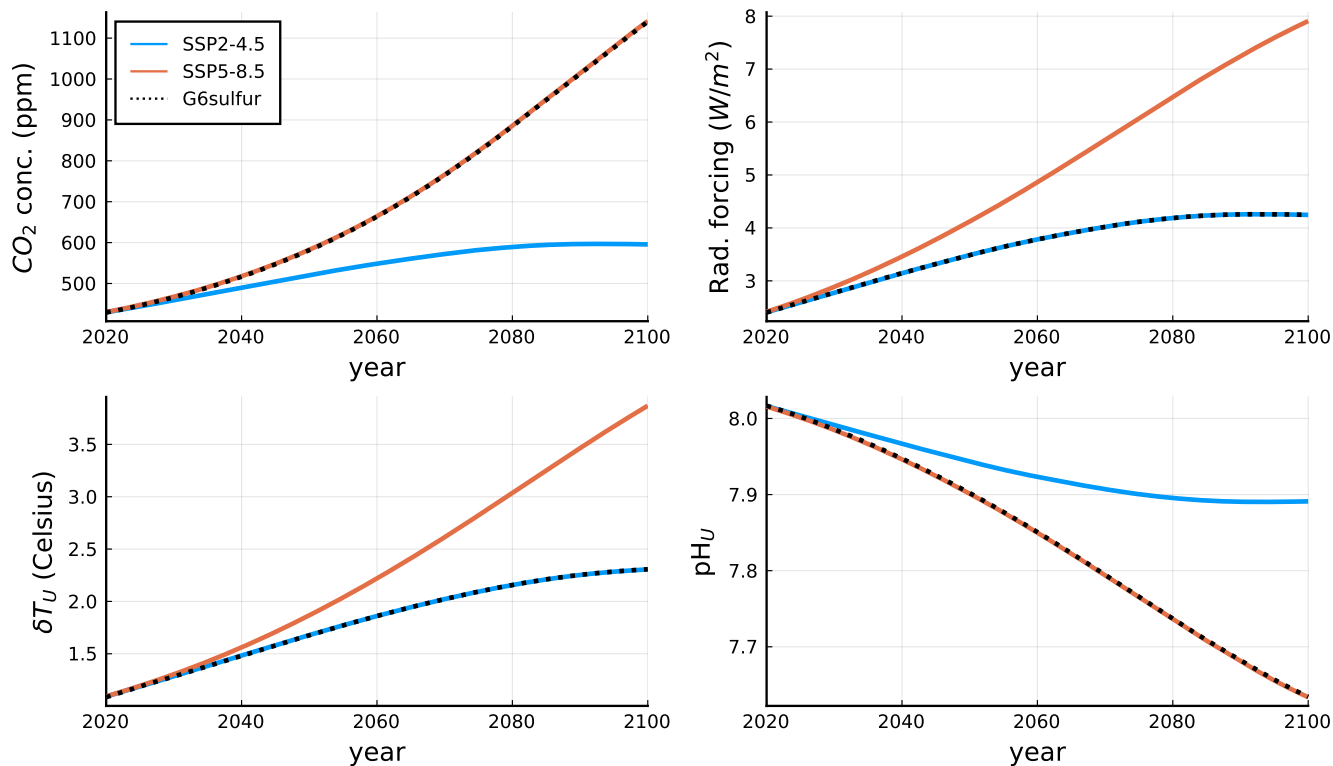
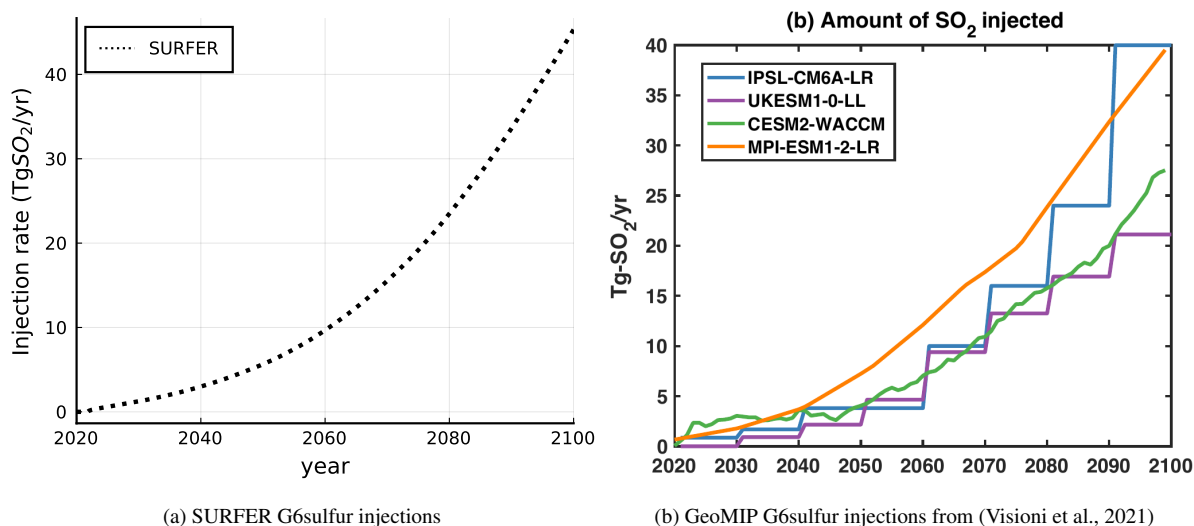


Figure 11. SURFER’s output for the G6sulfur experiment. From left to right, top to bottom: CO₂ concentration, radiative forcing, temperature anomaly and pH in upper ocean layer.



(a) SURFER G6sulfur injections

(b) GeoMIP G6sulfur injections from (Visoni et al., 2021)

Figure 12. Comparison of aerosol injection rate needed to do the G6sulfur experiment by SURFER (left) and by some ESMs participating in GeoMIP (right).



emissions from thawed permafrost were not explored. In the ZECMIP experiments (Jones et al., 2019; MacDougall et al., 2020), only two of the models (NorESM2-LM and UVicESCM2.10) had a permafrost module. The presence of the module in these models is visible on the absolute size of their land carbon reservoir compared to the other models (see Figs. 5 and 6), but not on the evolution of the land reservoir anomalies, suggesting that, in these models at least, the permafrost feedback does not dominate other carbon fluxes. Burke et al. (2020) acknowledges that modelling future permafrost thaw and its resulting CO₂ emissions remains a challenge to ESMs and EMICs, and points to deeper soils and the inclusion of a representation of abrupt thawing events as the main points to be improved. For this reason we left the addition of this reservoir and its possible feedbacks for the future.

The value of the equilibrium climate sensitivity used in SURFER is compatible with that obtained by ESMs that include the effect of ice-albedo feedback from the melting of sea-ice. Consequently, the ice-albedo feedback coming from sea-ice can be thought of as already included in SURFER even if sea-ice is not explicitly part of the model. A representation of the ice-albedo feedback due to the melting of the ice sheets, however, is missing in SURFER. Wunderling et al. (2020) studied the impact of the melting of several cryosphere elements on the global mean temperature. They found that the full melting of Greenland's ice sheet would lead to a temperature increase of 0.13°C. Approximately 50% of which corresponds to albedo, and the rest to changes in lapse rate, water vapour and clouds. For the west Antarctic ice sheet an increase in temperature of 0.05°C was found, again with 50% of it coming from albedo effects. The East Antarctic ice sheet was not included in the study. Adding these effects has been left for future work in which more data from geographically-explicit models becomes available.

SURFER's carbon cycle does not take into account the soft tissue or the carbonate pump which act to create a Dissolved Inorganic Carbon gradient in the water column with the deeper layer containing more DIC than the upper layer. We have introduced a constant parameter, δ_{DIC} , which allows for this difference in DIC between layers to be captured. The soft tissue and carbonate pumps might be affected by temperature and CO₂ concentration changes, leading to a time evolving δ_{DIC} , while in SURFER this parameter remains constant.

The feedback of temperature on the physical component of the carbon cycle can be included by substituting the solubility constant K_0 and the dissociation constants K_1 and K_2 by their temperature dependent expressions as done in Glotter et al. (2014). This feedback, which acts in the direction of increasing atmospheric CO₂ by reducing the ocean carbon uptake, is however known to be small (Glotter et al., 2014) due to two competing processes; while solubility decreases with temperature, the dissociation constants increase.

Calcium carbonate compensation, a slower process in which the ocean's pH is neutralised by the dissolution of CaCO₃ from sediments is not present in SURFER. Calcium carbonate compensation acts on timescales of 3-7 kyr (Archer et al., 2009) and provides an extra buffer for atmospheric CO₂. Since the impact from ocean acidification on marine ecosystems takes place at much shorter timescales, and since the highest and most harmful rates of sea level rise occur before the year 4000 for the RCP scenarios, it seems unnecessary for our purposes to add this effect (together with a sediments reservoir) into SURFER. Due to this choice its predictions will start to deviate from expected on timescales of several thousands of years and ocean acidification will be slightly intensified with respect to models which do include such processes. We have also ignored even longer timescale effects related to the CO₂ chemical reaction with silicate rocks.



In SURFER, the impact solar radiation management with sulfur dioxide is exerted only on the globally averaged temperature. The focus on temperature may implicitly cause an under-appreciation of the risks associated with this or similar solar radiation management technologies, especially their direct impacts on atmospheric chemistry, circulation, precipitation and their indirect impacts on health and food security. As already stated in the introduction, this inclusion is motivated by the need to put in a single coherent framework the contrasting timescales of the (short) residence time of stratospheric aerosols, the (long) residence time of carbon in the ocean-atmosphere system and the timescales involved in the sea-level response. We nevertheless urge potential users of SURFER interested in evaluating the cost and benefits and related dilemmas associated with solar radiation management to adequately incorporate its potentially severe adverse side effects in their studies and conclusions. Solar radiation management impacts cannot be reduced to temperature and any study considering this technology as an option should account for the multifaceted risks associated with it (Robock, 2016). Not doing so will likely lead to bad and dangerous advice.

5 Conclusions

Most policy analyses in the context of climate change and climate policy focus on the next decades to a couple of hundreds of years. It is reasonable to ask ourselves what are the best decisions to be made in the next decades as opposed to those to be made in the next millennia. What is not reasonable is to ignore the long-term consequences of such short-term decisions in assessments. Science has shown that anthropogenic emissions have very long-term effects, not only on the temperature but also on ocean acidification and especially on sea level rise.

Moreover, they tend to focus solely on temperature, ignoring ocean acidification, sea level rise and tipping points. Here we presented SURFER, a carbon, climate, sea level rise model which is very fast and simple to use. Due to its lightness and ability to correctly represent longer timescales, ocean acidification and sea level rise (from ice sheet tipping points), it is well-suited for long-sighted multi-objective policy analyses: With this model we can not only assess the short and long-term effects of anthropogenic emissions, but also put future technologies into the mix, such as carbon dioxide removal and solar radiation management.

The ice sheet part of the model can easily be updated to match latest research on ice sheet tipping points. In particular, one could decide to model Antarctica with two separate ice sheets, one for the West Antarctic Ice Sheet (more susceptible) and one for the East Antarctic Ice Sheet (more resilient). Likewise, the equation for the land reservoir can readily be adapted to the latest results as they become available.

SURFER is rich enough to adequately describe a number of features that should be considered when assessing the impacts of different policies and, as was shown here, it behaves well under a big spectrum of emission scenarios.

Code availability. The exact version of SURFER used to produce the results used in this paper is archived on Zenodo (Martínez Montero et al., 2022) under MIT license, as is the input data to run the model and produce the plots for all the simulations presented in this paper.



Author contributions. Based on pertinent roles defined by CASRAI's CRediT – Contributor Roles Taxonomy: Conceptualization (MM, MC, NB, NB), Methodology (MM, MC, VC), Project Administration (MC), Software (MM), Supervision (MC), Validation (MM), Visualization (MM, NuriaB), Writing – original draft (MM), Writing – review & editing (MC, NB, NB, VC).

Competing interests. None

490 *Acknowledgements.* This project is TiPES contribution #146: This project has received funding from the European Union's Horizon 2020 research and innovation programme under grant agreement No 820970". MC is funded as Research Director by the Belgian National Fund of Scientific Research. VC is funded as Research Fellow by the Belgian National Fund of Scientific Research (F.S.R.-FNRS)".



References

- Archer, D.: Fate of fossil fuel CO₂ in geologic time, *Journal of Geophysical Research C: Oceans*, 110, 1–6, <https://doi.org/10.1029/2004JC002625>, 2005.
- Archer, D., Eby, M., Brovkin, V., Ridgwell, A., Cao, L., Mikolajewicz, U., Caldeira, K., Matsumoto, K., Munhoven, G., Montenegro, A., and Tokos, K.: Atmospheric Lifetime of Fossil Fuel Carbon Dioxide, *Annual Review of Earth and Planetary Sciences*, 37, 117–134, <https://doi.org/10.1146/annurev.earth.031208.100206>, 2009.
- Arias, P.A., Bellouin, N., Coppola, E., Jones, R., Krinner, G., Marotzke, J., Naik, V., Palmer, M., Plattner, G.-K., Rogelj, J., Rojas, M., Sillmann, J., Storelvmo, T., Thorne, P., Trewin, B., Rao, K. A., Adhikary, B., Allan, R., Armour, K., Bala, G., Barimalala, R., Berger, S., Canadell, J., Cassou, C., Cherchi, A., Collins, W., Collins, W., Connors, S., Corti, S., Cruz, F., Dentener, F., Dereczynski, C., Luca, A. D., Niang, A. D., Doblus-Reyes, F., Dosio, A., Douville, H., Engelbrecht, F., Eyring, V., Fischer, E., Forster, P., Fox-Kemper, B., Fuglested, J., Fyfe, J., Gillett, N., Goldfarb, L., Gorodetskaya, I., Gutierrez, J., Hamdi, R., Hawkins, E., Hewitt, H., Hope, P., Islam, A., Jones, C., Kaufman, D., Kopp, R., Kosaka, Y., Kossin, J., Krakovska, S., Lee, J.-Y., Li, J., Mauritsen, T., Maycock, T., Meinshausen, M., Min, S.-K., Monteiro, P., Ngo-Duc, T., Otto, F., Pinto, I., Pirani, A., Raghavan, K., Ranasinghe, R., Ruane, A., Ruiz, L., Sallée, J.-B., Samset, B., Sathyendranath, S., Seneviratne, S., Sörensson, A., Szopa, S., Takayabu, I., Tréguier, A.-M., van den Hurk, B., Vautard, R., von Schuckmann, K., Zaehle, S., Zhang, X., and Zickfeld, K.: 2021: Technical Summary. In *Climate Change 2021: The Physical Science Basis. Contribution of Working Group I to the Sixth Assessment Report of the Intergovernmental Panel on Climate Change* [Masson-Delmotte, V., P. Zhai, A. Pirani, S.L. Connors, C. Péan, S. Berger, N. Caud, Y. Chen, L. Goldfarb, M.I. Gomis, M. Huang, K. Leitzell, E. Lonnoy, J.B.R. Matthews, T.K. Maycock, T. Waterfield, O. Yelekçi, R. Yu, and B. Zhou (eds.)]. Cambridge University Press. In Press., 2021.
- Bezanson, J., Edelman, A., Karpinski, S., and Shah, V. B.: Julia: A Fresh Approach to Numerical Computing, *SIAM Review*, 59, 65–98, <https://doi.org/10.1137/141000671>, 2017.
- Bolin, B. and Eriksson, E.: Changes in the Carbon Dioxide Content of the Atmosphere and Sea due to Fossil Fuel Combustion, *The atmosphere and the sea in motion*, pp. 130–142, http://climatepositions.com/wp-content/uploads/2014/03/n8._Bolin___Eriksson__1958corrected.pdf, 1959.
- Burke, E. J., Ekici, A., Huang, Y., Chadburn, S. E., Huntingford, C., Ciais, P., Friedlingstein, P., Peng, S., and Krinner, G.: Quantifying uncertainties of permafrost carbon-climate feedbacks, *Biogeosciences*, 14, 3051–3066, <https://doi.org/10.5194/bg-14-3051-2017>, 2017.
- Burke, E. J., Zhang, Y., and Krinner, G.: Evaluating permafrost physics in the Coupled Model Intercomparison Project 6 (CMIP6) models and their sensitivity to climate change, *Cryosphere*, 14, 3155–3174, <https://doi.org/10.5194/tc-14-3155-2020>, 2020.
- Canadell, J.G., Monteiro, P. M. S., Costa, M. H., Cotrim da Cunha, L., Cox, P. M., Eliseev, A. V., Henson, S., Ishii, M., Jaccard, S., Koven, C., Lohila, A., Patra, P. K., Piao, S., Rogelj, J., Syampungani, S., Zaehle, S., and Zickfeld, K.: 2021: Global Carbon and other Biogeochemical Cycles and Feedbacks. In *Climate Change 2021: The Physical Science Basis. Contribution of Working Group I to the Sixth Assessment Report of the Intergovernmental Panel on Climate Change* [Masson-Delmotte, V., P. Zhai, A. Pirani, S.L. Connors, C. Péan, S. Berger, N. Caud, Y. Chen, L. Goldfarb, M.I. Gomis, M. Huang, K. Leitzell, E. Lonnoy, J.B.R. Matthews, T.K. Maycock, T. Waterfield, O. Yelekçi, R. Yu, and B. Zhou (eds.)]. Cambridge University Press. In Press., 2021.
- Carlino, A., Giuliani, M., Tavoni, M., and Castelletti, A.: Multi-objective optimal control of a simple stochastic climate-economy model, *IFAC-PapersOnLine*, 53, 16 593–16 598, <https://doi.org/10.1016/j.ifacol.2020.12.786>, 2020.



- Chadburn, S. E., Burke, E. J., Cox, P. M., Friedlingstein, P., Hugelius, G., and Westermann, S.: An observation-based constraint on permafrost
530 loss as a function of global warming, *Nature Climate Change*, 7, 340–344, <https://doi.org/10.1038/nclimate3262>, 2017.
- Clark, P. U., Shakun, J. D., Marcott, S. A., Mix, A. C., Eby, M., Kulp, S., Levermann, A., Milne, G. A., Pfister, P. L., Santer, B. D.,
Schrag, D. P., Solomon, S., Stocker, T. F., Strauss, B. H., Weaver, A. J., Winkelmann, R., Archer, D., Bard, E., Goldner, A., Lambeck, K.,
Pierrehumbert, R. T., and Plattner, G. K.: Consequences of twenty-first-century policy for multi-millennial climate and sea-level change,
Nature Climate Change, 6, 360–369, <https://doi.org/10.1038/nclimate2923>, 2016.
- 535 Garbe, J., Albrecht, T., Levermann, A., Donges, J. F., and Winkelmann, R.: The hysteresis of the Antarctic Ice Sheet, *Nature*, 585, 538–544,
<https://doi.org/10.1038/s41586-020-2727-5>, 2020.
- Gardiner, S. M.: Is “Arming the Future” with Geoengineering Really the Lesser Evil? Some doubts about the ethics of intentionally manipu-
lating the climate system. In *Climate Ethics: Essential Readings*, <https://doi.org/10.1093/oso/9780195399622.001.0001>, 2010.
- Glotter, M. J., Pierrehumbert, R. T., Elliott, J. W., Matteson, N. J., and Moyer, E. J.: A simple carbon cycle representation for economic and
540 policy analyses, *Climatic Change*, 126, 319–335, <https://doi.org/10.1007/s10584-014-1224-y>, 2014.
- Gregory, J., George, S., and Smith, R.: Large and irreversible future decline of the Greenland ice-sheet, *The Cryosphere Discussions*, pp.
1–28, <https://doi.org/10.5194/tc-2020-89>, 2020.
- Gregory, J. M.: Vertical heat transports in the ocean and their effect on time-dependent climate change, *Climate Dynamics*, 16, 501–515,
<https://doi.org/10.1007/s003820000059>, 2000.
- 545 Gutiérrez, J.M., Jones, R., Narisma, G., Alves, L., Amjad, M., Gorodetskaya, I., Grose, M., Klutse, N., Krakovska, S., Li, J., Martínez-Castro,
D., Mearns, L., Mernild, S., Ngo-Duc, T., van den Hurk, B., , and Yoon, J.-H.: 2021: Atlas. In *Climate Change 2021: The Physical Science
Basis. Contribution of Working Group I to the Sixth Assessment Report of the Intergovernmental Panel on Climate Change [Masson-
Delmotte, V., P. Zhai, A. Pirani, S.L. Connors, C. Péan, S. Berger, N. Caud, Y. Chen, L. Goldfarb, M.I. Gomis, M. Huang, K. Leitzell, E.
Lonnoy, J.B.R. Matthews, T.K. Maycock, T. Waterfield, O. Yelekçi, R. Yu, and B. Zhou (eds.)]*, 2021.
- 550 Hänsel, M. C., Drupp, M. A., Johansson, D. J., Nesje, F., Azar, C., Freeman, M. C., Groom, B., and Sterner, T.: Climate economics support
for the UN climate targets, *Nature Climate Change*, 10, 781–789, <https://doi.org/10.1038/s41558-020-0833-x>, 2020.
- Held, I. M., Winton, M., Takahashi, K., Delworth, T., Zeng, F., and Vallis, G. K.: Probing the fast and slow components of global warming
by returning abruptly to preindustrial forcing, *Journal of Climate*, 23, 2418–2427, <https://doi.org/10.1175/2009JCLI3466.1>, 2010.
- Helwegen, K. G., Wieners, C. E., Frank, J. E., and Dijkstra, H. A.: Complementing CO₂ emission reduction by solar radiation management
555 might strongly enhance future welfare, *Earth System Dynamics*, 10, 453–472, <https://doi.org/10.5194/esd-10-453-2019>, 2019.
- Huybrechts, P.: Glaciological Modelling of the Late Cenozoic East Antarctic Ice Sheet: Stability or Dynamism?, *Geografiska Annaler: Series
A, Physical Geography*, 75, 221–238, <https://doi.org/10.1080/04353676.1993.11880395>, 1993.
- Jones, C. D., Frölicher, T. L., Koven, C., MacDougall, A. H., Damon Matthews, H., Zickfeld, K., Rogelj, J., Tokarska, K. B., Gillett, N. P.,
Ilyina, T., Meinshausen, M., Mengis, N., Séférian, R., Eby, M., and Burger, F. A.: The Zero Emissions Commitment Model Intercompar-
560 ison Project (ZECMIP) contribution to C4MIP: Quantifying committed climate changes following zero carbon emissions, *Geoscientific
Model Development*, 12, 4375–4385, <https://doi.org/10.5194/gmd-12-4375-2019>, 2019.
- Keen, S.: The appallingly bad neoclassical economics of climate change, *Globalizations*, pp. 1–33,
<https://doi.org/10.1080/14747731.2020.1807856>, 2020.
- Keen, S., Lenton, T. M., Godin, A., Yilmaz, D., Grasselli, M., and Garrett, T. J.: Economists’ erroneous estimates of damages from climate
565 change, <http://arxiv.org/abs/2108.07847>, 2021.



- Kravitz, B., Robock, A., Tilmes, S., Boucher, O., English, J. M., Irvine, P. J., Jones, A., Lawrence, M. G., MacCracken, M., Muri, H., Moore, J. C., Niemeier, U., Phipps, S. J., Sillmann, J., Storelvmo, T., Wang, H., and Watanabe, S.: The Geoengineering Model Inter-comparison Project Phase 6 (GeoMIP6): Simulation design and preliminary results, *Geoscientific Model Development*, 8, 3379–3392, <https://doi.org/10.5194/gmd-8-3379-2015>, 2015.
- 570 Kwiatkowski, L., Torres, O., Bopp, L., Aumont, O., Chamberlain, M., Christian, J., Dunne, J., Gehlen, M., Ilyina, T., John, J., Lenton, A., Li, H., Lovenduski, N., Orr, J., Palmieri, J., Schwinger, J., Séférian, R., Stock, C., Tagliabue, A., Takano, Y., Tjiputra, J., Toyama, K., Tsujino, H., Watanabe, M., Yamamoto, A., Yool, A., and Ziehn, T.: Twenty-first century ocean warming, acidification, deoxygenation, and upper ocean nutrient decline from CMIP6 model projections, *Biogeosciences Discussions*, pp. 1–43, <https://doi.org/10.5194/bg-2020-16>, 2020.
- Lenton, T. M., Held, H., Kriegler, E., Hall, J. W., Lucht, W., Rahmstorf, S., and Schellnhuber, H. J.: Tipping elements in the Earth's climate system, *Proceedings of the National Academy of Sciences*, 105, 1786–1793, <https://doi.org/10.1073/pnas.0705414105>, 2008.
- 575 Letreguilly, A., Huybrechts, P., and Reeh, N.: Steady-state characteristics of the Greenland ice sheet under different climates, *Journal of Glaciology*, 37, 149–157, <https://doi.org/10.1017/S0022143000042908>, 1991.
- MacDougall, A. H. and Knutti, R.: Projecting the release of carbon from permafrost soils using a perturbed parameter ensemble modelling approach, *Biogeosciences*, 13, 2123–2136, <https://doi.org/10.5194/bg-13-2123-2016>, 2016.
- 580 MacDougall, A. H., Frölicher, T. L., Jones, C. D., Rogelj, J., DamonMatthews, H., Zickfeld, K., Arora, V. K., Barrett, N. J., Brovkin, V., Burger, F. A., Eby, M., Eliseev, A. V., Hajima, T., Holden, P. B., Jeltsch-Thömmes, A., Koven, C., Mengis, N., Menviel, L., Michou, M., Mokhov, I. I., Oka, A., Schwinger, J., Séférian, R., Shaffer, G., Sokolov, A., Tachiiri, K., Tjiputra, J., Wiltshire, A., and Ziehn, T.: Is there warming in the pipeline? A multi-model analysis of the Zero Emissions Commitment from CO₂, *Biogeosciences*, 17, 2987–3016, <https://doi.org/10.5194/bg-17-2987-2020>, 2020.
- 585 Martínez Montero, M., Crucifix, M., Couplet, V., Brede, N., and Botta, N.: SURFER v1.0.0, <https://doi.org/10.5281/zenodo.6406224>, 2022.
- Meinshausen, M., Smith, S. J., Calvin, K., Daniel, J. S., Kainuma, M. L., Lamarque, J., Matsumoto, K., Montzka, S. A., Raper, S. C., Riahi, K., Thomson, A., Velders, G. J., and van Vuuren, D. P.: The RCP greenhouse gas concentrations and their extensions from 1765 to 2300, *Climatic Change*, 109, 213–241, <https://doi.org/10.1007/s10584-011-0156-z>, 2011.
- Meinshausen, M., Nicholls, Z. R. J., Lewis, J., Gidden, M. J., Vogel, E., Freund, M., Beyerle, U., Gessner, C., Nauels, A., Bauer, N., Canadell, J. G., Daniel, J. S., John, A., Krummel, P. B., Luderer, G., Meinshausen, N., Montzka, S. A., Rayner, P. J., Reimann, S., Smith, S. J., van den Berg, M., Velders, G. J. M., Vollmer, M. K., and Wang, R. H. J.: The shared socio-economic pathway (SSP) greenhouse gas concentrations and their extensions to 2500, *Geoscientific Model Development*, 13, 3571–3605, <https://doi.org/10.5194/gmd-13-3571-2020>, 2020.
- 590 Moreno-Cruz, J. B. and Keith, D. W.: Climate policy under uncertainty: A case for solar geoengineering, *Climatic Change*, 121, 431–444, <https://doi.org/10.1007/s10584-012-0487-4>, 2013.
- 595 Moss, R. H., Edmonds, J. A., Hibbard, K. A., Manning, M. R., Rose, S. K., Van Vuuren, D. P., Carter, T. R., Emori, S., Kainuma, M., Kram, T., Meehl, G. A., Mitchell, J. F., Nakicenovic, N., Riahi, K., Smith, S. J., Stouffer, R. J., Thomson, A. M., Weyant, J. P., and Wilbanks, T. J.: The next generation of scenarios for climate change research and assessment, *Nature*, 463, 747–756, <https://doi.org/10.1038/nature08823>, 2010.
- Niemeier, U. and Timmreck, C.: What is the limit of climate engineering by stratospheric injection of SO₂?, *Atmospheric Chemistry and Physics*, 15, 9129–9141, <https://doi.org/10.5194/acp-15-9129-2015>, 2015.
- 600 Nordhaus, W. D.: The 'DICE' Model: Background and Structure of a Dynamic Integrated Climate-Economy Model of the Economics of Global Warming, <http://ideas.repec.org/p/cwl/cwldpp/1009.html>, 1992.



- Nordhaus, W. D.: DICE 2013R: Introduction and User's Manual, Yale University Press, p. 102, http://www.econ.yale.edu/~simon/nordhaus/homepage/homepage/documents/DICE_Manual_100413r1.pdf, 2013.
- 605 Pattyn, F.: GRANTISM: An Excel™ model for Greenland and Antarctic ice-sheet response to climate changes, *Computers and Geosciences*, 32, 316–325, <https://doi.org/10.1016/j.cageo.2005.06.020>, 2006.
- Ridley, J., Gregory, J. M., Huybrechts, P., and Lowe, J.: Thresholds for irreversible decline of the Greenland ice sheet, *Climate Dynamics*, 35, 1065–1073, <https://doi.org/10.1007/s00382-009-0646-0>, 2010.
- Robinson, A., Calov, R., and Ganopolski, A.: Multistability and critical thresholds of the Greenland ice sheet, *Nature Climate Change*, 2, 610 429–432, <https://doi.org/10.1038/nclimate1449>, 2012.
- Robock, A.: Albedo enhancement by stratospheric sulfur injections: More research needed, *Earth's Future*, 4, 644–648, <https://doi.org/10.1002/2016EF000407>, 2016.
- Rockström, J., Steffen, W., Noone, K., Persson, Å., Chapin, F. S., Lambin, E. F., Lenton, T. M., Scheffer, M., Folke, C., Schellnhuber, H. J., Nykvist, B., de Wit, C. A., Hughes, T., van der Leeuw, S., Rodhe, H., Sörlin, S., Snyder, P. K., Costanza, R., Svedin, U., Falkenmark, 615 M., Karlberg, L., Corell, R. W., Fabry, V. J., Hansen, J., Walker, B., Liverman, D., Richardson, K., Crutzen, P., and Foley, J. A.: A safe operating space for humanity, *Nature*, 461, 472–475, <https://doi.org/10.1038/461472a>, 2009.
- Sarmiento, J. and Gruber, N.: *Ocean Biogeochemical Dynamics*, Princeton University Press, <https://press.princeton.edu/books/hardcover/9780691017075/ocean-biogeochemical-dynamics>, 2006.
- Steffen, W., Richardson, K., Rockstrom, J., Cornell, S. E., Fetzer, I., Bennett, E. M., Biggs, R., Carpenter, S. R., de Vries, W., de Wit, C. A., 620 Folke, C., Gerten, D., Heinke, J., Mace, G. M., Persson, L. M., Ramanathan, V., Reyers, B., and Sorlin, S.: Planetary boundaries: Guiding human development on a changing planet, *Science*, 347, 1259 855–1259 855, <https://doi.org/10.1126/science.1259855>, 2015.
- Turetsky, M. R., Abbott, B. W., Jones, M. C., Anthony, K. W., Olefeldt, D., Schuur, E. A., Grosse, G., Kuhry, P., Hugelius, G., Koven, C., Lawrence, D. M., Gibson, C., Sannel, A. B. K., and McGuire, A. D.: Carbon release through abrupt permafrost thaw, *Nature Geoscience*, 13, 138–143, <https://doi.org/10.1038/s41561-019-0526-0>, 2020.
- 625 Van Breedam, J., Goelzer, H., and Huybrechts, P.: Semi-equilibrated global sea-level change projections for the next 10 000 years, *Earth System Dynamics*, 11, 953–976, <https://doi.org/10.5194/esd-11-953-2020>, 2020.
- Visioni, D., MacMartin, D., Kravitz, B., Boucher, O., Jones, A., Lurton, T., Martine, M., Mills, M., Nabat, P., Niemeier, U., Séférian, R., and Tilmes, S.: Identifying the sources of uncertainty in climate model simulations of solar radiation modification with the G6sulfur and G6solar Geoengineering Model Intercomparison Project (GeoMIP) simulations, *Atmospheric Chemistry and Physics*, pp. 1–37, 630 <https://doi.org/10.5194/acp-2021-133>, 2021.
- Wunderling, N., Willeit, M., Donges, J. F., and Winkelmann, R.: Global warming due to loss of large ice masses and Arctic summer sea ice, *Nature Communications*, 11, 1–8, <https://doi.org/10.1038/s41467-020-18934-3>, 2020.